

EVALUATION OF BULK CHARGING IN GEOSTATIONARY TRANSFER ORBIT AND EARTH ESCAPE TRAJECTORIES USING THE NUMIT 1-D CHARGING MODEL

Joseph I. Minow and Victoria N. Coffey

NASA, Marshall Space Flight Center, Huntsville, Alabama 35812 (USA)

Linda N. Parker, William C. Blackwell, Jr.

Jacobs Engineering, ESTS Group, Huntsville, Alabama 35812 (USA)

Insoo Jun and Henry B. Garrett

The Jet Propulsion Laboratory, The California Institute of Technology,
4800 Oak Grove Drive, Pasadena, California, 91109 (USA)

ABSTRACT: *The NUMIT 1-dimensional bulk charging model is used as a screening tool for evaluating time-dependent bulk (internal or deep dielectric) charging of dielectrics exposed to penetrating electron environments. The code is modified to accept time dependent electron flux time series along satellite orbits for the electron environment inputs instead of using the static electron flux environment input originally used by the code and widely adopted in bulk charging models.*

Application of the screening technique is demonstrated for three cases of spacecraft exposure within the Earth's radiation belts including a geostationary transfer orbit and an Earth-Moon transit trajectory for a range of orbit inclinations. Electric fields and charge densities are computed for dielectric materials with varying electrical properties exposed to relativistic electron environments along the orbits. Our objective is to demonstrate a preliminary application of the time-dependent environments input to the NUMIT code for evaluating charging risks to exposed dielectrics used on spacecraft when exposed to the Earth's radiation belts. The results demonstrate that the NUMIT electric field values in GTO orbits with multiple encounters with the Earth's radiation belts are consistent with previous studies of charging in GTO orbits and that potential threat conditions for electrostatic discharge exist on lunar transit trajectories depending on the electrical properties of the materials exposed to the radiation environment.

1 - INTRODUCTION

Spacecraft orbiting the Earth within approximately 10 Earth radii, on transfer orbits to the Moon at 60 Earth radii, or Earth escape trajectories to deep space destinations beyond the Moon will be exposed to the surface and bulk (internal or deep dielectric) charging environments due to energetic electrons trapped within the Earth's radiation belts. Spacecraft charging results from the differential collection of electron and ion currents on or in spacecraft materials when exposed to space plasma and radiation environments. Accumulation of a net negative charge density on spacecraft surfaces (surface charging) and buried inside insulators (bulk charging) generate electric potentials and fields. Electrostatic discharge (ESD) arcs occur when the electric fields associated with the potential gradients exceed the breakdown strength of the insulating materials. ESD is a well known source of spacecraft anomalies and failures. Table 1 demonstrates that over half the space system anomalies attributed to the space environment are due to ESD and bulk charging accounts for the majority of the ESD related spacecraft anomalies. Bulk charging has been implicated in satellite anomalies in geostationary orbit [Wrenn, 1995] and pulsing (arcing) of dielectrics has been well characterized in geostationary transfer orbits using data from the Internal Discharge Monitor on the Combined Radiation and Release Experiment Satellite (CRRES) to show that pulsing of thinly shielded samples of highly resistive dielectrics materials is strongly correlated with the increase in relativistic electron flux along the orbit [Frederickson et al., 1992; 1992; Frederickson, 1996; Violet and Frederickson, 1993]. In addition, examples of spacecraft lost or missions terminated due to charging (either surface or bulk) include the DSDC II, GOES 4, Feng Yun 1, MARECS A, Anik E2, Telstar 401, and INSAT 2D spacecraft [Koons et al., 2000] with the recent failure of the ADEOS-II spacecraft in 2003 [Kawakita et al., 2005].

The spacecraft anomaly or failure mechanism is attributed to arcs and transient high current pulses originating in insulators charged to large negative potentials when exposed to space plasma and radiation environments. Figure 1 is an example of electrostatic discharge damage in an acrylic block following exposure to electrons accelerated to a few million electron volts (MeV) by a laboratory accelerator. Although the MeV electrons only have sufficient energy to penetrate about a centimeter into the acrylic insulating material, the damage produced by the ESD arc originating in the charged region of the polymer extends nearly the full 10 cm width of the acrylic block.

Table 1. Environment Impacts on Space Systems*

Anomaly Diagnosis	Number	%
ESD-Bulk charging	74	24.7
ESD-Surface charging	59	19.7
ESD-Uncategorized	29	9.7
Single event upsets	85	28.4
Radiation Dose	16	5.4
Micrometeoroids, orbital debris	10	3.3
Atomic oxygen	1	0.3
Atmospheric drag	1	0.3
Other	24	8.0
Total	299	100.0%

ESD damage to materials is a potential safety hazard to manned space flight systems relying on insulating materials for critical system components when they are exposed to the MeV electron environments in the Earth's radiation belts or generated during transient solar energetic particle events. For example, polymer composite spacecraft hulls, lightweight structural materials, multi-functional polymeric radiation shielding, thermal protection materials, and polymer signal and power cable insulation are all examples of insulating materials used for mission critical components on spacecraft which are susceptible to ESD degradation. In addition to the materials issues, a

serious risk to spacecraft systems are the transient currents generated by the ESD arcs which can couple to avionics systems creating anomalous system commands including anomalous thruster firings, logic errors in control device memories, and phantom commands to attitude control devices. In the worst case the currents can even completely destroy sensitive electronic components resulting in system failure or mission loss. In addition to the materials and electronics issues, charging can be detrimental to the operation of space science instrumentation on robotic probes when spacecraft potentials perturb the incoming radiation fields to such a degree that sensitive instruments designed to monitor the environment no longer are able to sample free field radiation environments.

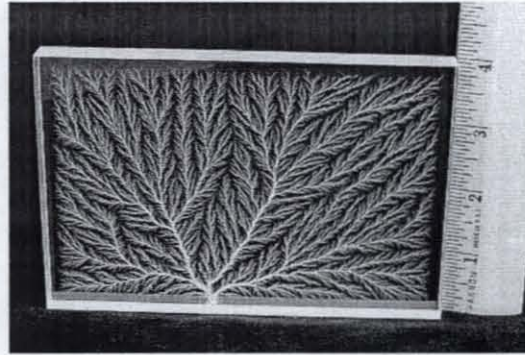


Figure 1. Electrostatic discharge damage in acrylic following exposure to MeV electrons (image courtesy of Bert Hickman, <http://www.teslamania.com>, 2007).

Negative spacecraft potentials in low Earth orbit range from only about a volt in low inclination orbits to a few hundred volts or even few thousand volts in high inclination orbits that pass through the Earth's auroral zone. More extreme spacecraft potentials are observed in the Earth's outer electron radiation belts where spacecraft in geostationary orbit, geostationary transfer orbit, and even earth escape trajectories through the radiation belts may charge to kilovolt potentials and in some extreme cases even tens of kilovolts. Charging is an issue that will have to be addressed for future lunar missions because human transport, cargo, and research vehicles will have to traverse the harsh charging regimes of the Earth's radiation belts on the way to and from the Moon. In addition, there is recent evidence from the Lunar Prospector spacecraft in a 30 km altitude orbit about the Moon suggesting lunar surface potentials of a few hundred to few thousand volts are possible in the dark regions of the lunar plasma wake when the Moon is inside the Earth's magnetotail [Halekas et al., 2005, 2007]. Charging of space systems exposed to space radiation environments both in low lunar orbit and on the surface of the Moon will certainly need to be evaluated for future lunar programs.

Procedures for building space systems to safely and reliably operate in charging environments is accomplished through a design process that includes implementing hardware construction techniques to meet spacecraft charging design guidelines, evaluation of spacecraft design and materials selection to determine the magnitude of potentials and fields that will be generated during exposure to space environments, and verification that insulating materials chosen for the system will not accumulate sufficient charge to arc while exposed to the most extreme space radiation environment during the vehicle's mission. The most cost effective method of conducting the evaluation and verification steps is to model the electrical response of the spacecraft or spacecraft materials to exposure to space radiation environments because trades on materials and environments can be easily conducted in the simulation environment. Laboratory testing is often used for final testing and for measuring the electrical properties of materials required for inputs to the charging codes. Even if laboratory testing is employed in the design and verification process, an analytical charging model is required to design, implement, and evaluate credible test programs which adequately reproduce the operational environment in space.

This paper describes an application of the NUMIT 1-D bulk charging model for use in screening dielectric materials for potential bulk charging risk during exposure to energetic electron environments. We first describe the bulk charging model, materials, and environments used for input to the charging code. Next, charging results for materials are given for spacecraft orbits including a geostationary transfer orbit (GTO) and an Earth-Moon lunar transit trajectory exposed

to mean solar maximum electron environments. Finally, we consider examples of material exposure to more extreme environments along the lunar transit orbit.

2 - MODEL

The NUMIT (for “numerical integration”) bulk charging model [Frederickson, 1974; 1983] has been used extensively for evaluating laboratory exposure of insulators to energetic electrons and scientific studies of space flight ESD experiments including a successful application to the CRRES IDM in-situ charging experiments [Frederickson, 1980; Frederickson and Brautigam, 2004]. Details of the model are described by Frederickson et al. [refs] and more recently by Jun et al. [2007] and only a brief description will be presented here.

2.1 – NUMIT MODEL AND ENVIRONMENTS

The NUMIT model is a finite difference solution to the bulk charging equation set [c.f., Sessler, 1987; Sessler et al., 2004]

$$\nabla \cdot E = -\nabla^2 \Phi = \frac{\rho}{\kappa \epsilon_0} \quad [1.]$$

$$\frac{\partial \rho}{\partial t} = -\nabla \cdot (J_R + J_C) \quad [2.]$$

where ρ is the charge density, Φ is the electric potential, J_R the space radiation current density, J_C the conduction current density in the insulator, and κ and ϵ_0 are the dielectric constant and permittivity of free space, respectively. Conduction currents are given by

$$J_C = \sigma E = \left[\sigma_{dark} + k_p \left(\frac{d\gamma}{dt} \right)^\alpha \right] E \quad [3.]$$

where σ is the bulk conductivity of the insulator which is often divided into two terms, the σ_{dark} conductivity in the absence of exposure to photons or charged particles and a radiation dose rate ($d\gamma/dt$) dependent term due to additional current carriers generated by interaction of the radiation field with the dielectric material. Numerical solution of equations (1) through (3) are accomplished using a 1-D finite difference approximation for spatial steps within the insulating material at successive time steps yielding values of the electric field, conduction currents, dose rates, and charge density as a function of depth in the material and time. The version of the code used here assumes a single planar dielectric between two grounded metal electrodes and the thickness of the first metal electrode is infinitely thin so there is no modification of the incident electron energy or flux as it passes through the electron [Jun et al., 2007]. Materials are divided into 60 spatial steps and time steps of 60 seconds are used for all of the results included in this report.

The original version of the NUMIT model provided time dependent output parameters for materials exposed to a constant radiation environment. We have modified the code to read input data files which provide the time step and electron flux at multiple energies. Electron flux data sets can either be derived from models of the space radiation environment or directly from satellite measurements in environments of interest to the user. This modified version of the code provides a capability of computing time dependent charging quantities in time varying electron environments. Because NUMIT uses a computationally efficient analytical approximation to transport the electron flux through the insulating material, estimate energy deposition (dose) by the radiation current, and evaluate electric charge deposition [Frederickson and Bell, 1995], there is little penalty in computational time to run very long electron flux time series. We have used the code to screen nine charging environments in interplanetary space using input time series that span nearly a complete

solar cycle at one hour time steps which require only moderately longer run times than the three day examples we present here at 60 second time steps.

The incident electron radiation currents J_R are obtained from the AE-8 trapped electron model [Vette, 1991]. AE-8 is recognized as a standard model for use in establishing radiation dose environments but has limitations for charging studies since it represents a long term mean

Table 2. Dielectric Material Properties

Parameter	Materials					
	1	2	3	4	5	6
Dark Conductivity (S/cm)	1×10^{-15}	1×10^{-17}	1×10^{-19}	2.19×10^{-18}	1×10^{-15}	1×10^{-18}
κ	3	3	3	4.48	3	3
Kp (S/m-rad-s ⁻¹)	3×10^{-16}	3×10^{-16}	3×10^{-16}	0	1×10^{-19}	1×10^{-19}
α	1.0	1.0	1.0	0	1.0	1.0
Molecular weight	38	38	38	38	38	38
Atomic number	19	19	19	19	19	19
Density (g/cm ³)	2.00	2.00	2.00	2.00	2.00	2.00
Thickness (cm)	1.00	1.00	1.00	1.00	1.00	1.00

environment for either solar minimum or solar maximum conditions and does not consider electron flux variations due to geomagnetic storms or solar wind interactions with the Earth's magnetosphere [c.f., Daly et al., 1996, 1999; Armstrong and Colburn, 2000; Lauenstein and Barth, 2005]. However, the AE-8 model provides a convenient method represent the mean electron flux environments that will be encountered during transit of the radiation belts. The Space Environment Information System (SPENVIS) toolset is used to establish both the spacecraft orbital ephemerides and the AE-8 electron integral flux environment along the orbit for this work. Spacecraft trajectories are computed for a three day period using the SPENVIS orbit propagator with a fixed perigee altitude of 250 km and varying apogee altitudes to establish the geostationary transfer orbit, lunar transit orbit, and deep space trajectories. Electron flux at the variable time steps provided by the SPENVIS models are interpolated onto a fixed 60 second time step. Electron flux along the resulting orbits are derived from the AE-8 solar maximum model for all cases presented in this paper to provide an estimate of the mean high electron flux environments during transit of the Earth's radiation belts. An additional case is given in Section 4.0 where the AE-8 outer electron belt environment has been enhanced by a factor of 10 to simulate a high flux geomagnetic storm environment.

2.2 – MATERIAL PROPERTIES

It is well known that charging behavior is strongly dependent on material properties of dielectric materials. A primary consideration in bulk charging is the volume conductivity which controls the rate at which excess electron charge deposited by the radiation currents from the space environment can leave the insulating material. The radiation induced conductivity parameters may not be as critical in low dose rate environments where the dark conductivity often dominates, but in high dose rate environments or at very low temperatures where the dark conductivity is greatly reduced the radiation induced conductivity may dominate.

For this study we adopt a set of representative values given in Table 2.0 which cover a range of insulating materials given in Table 1 of [4002 HDBK, Shugg, 1986]. Dielectric constants κ (where $\kappa = \epsilon/\epsilon_0$) of typical insulators used in spacecraft construction vary from minimum values of $\kappa \sim 2$ to

high values of $\kappa \sim 9$ while κ for most common polymer materials vary from 2 to 4. We adopt a representative value of $\kappa \sim 3$ here with a corresponding polymer density of 2 g/cm^3 . Standard design charging guidelines suggest limiting the DC volume conductivity of dielectric materials to values greater than 10^{-11} S/cm to 10^{-12} S/cm to avoid accumulation of excess charge [Purvis et al., 1984; 4002 HDBK]. However, it is not unusual for a variety of dielectrics to be used in spacecraft construction with DC volume conductivities ranging from $\sim 10^{-14} \text{ S/cm}$ to $>10^{-18} \text{ S/cm}$. We adopt a range of DC conductivities from the most conductive $\sigma \sim 10^{-15} \text{ S/cm}$ to a highly resistive material with $\sigma \sim 10^{-21} \text{ S/cm}$.

The choice of the highest conductivity that can be run by the model is constrained by noting that the charging time constant $\tau \sim \epsilon/\sigma$ must exceed at least a couple of the time steps used in the model for the results to avoid numerical instabilities. Using the 60 second time step, we find a maximum conductivity of $\sigma \sim \epsilon/\tau = (3 \cdot 8.85 \times 10^{-12} \text{ F/m}) / (60 \text{ s}) = 4.4 \times 10^{-13} \text{ S/m}$ and for the results presented here we choose $1 \times 10^{-13} \text{ S/m}$ for the limiting conductivity since it yields a time constant of $\tau \sim (3 \cdot 8.85 \times 10^{-12} \text{ F/m}) / (10^{-13} \text{ S/m}) = 265$ seconds for the shortest time constant. Evaluation of charging for greater conductivities is of course possible but the input environments will have to be specified at correspondingly smaller time steps to support the analysis. Volume conductivities for Material 2 and Material 3 are chosen to give charging time constants of approximately 2.5 hours and 31 days, respectively.

Radiation induced conductivity parameters of $k_p = 3 \times 10^{-16} \text{ S/m-rad-s}^{-1}$ and $\alpha=1$ are assumed for the first three materials [Frederickson, 1977; Frederickson and Brautigam, 2004]. Electrical properties of Material 4—an epoxy-fiberglass—have been measured by [Rodgers et al., 2003] and shown to have a negligible radiation induced conductivity. Materials 5 and 6 represent a material with small radiation induced conductivity independent of temperature, but a dark conductivity of 10^{-15} S/m at room temperature which is reduced by three orders of magnitude at $\sim 100\text{K}$. For the purpose of this work, we have simply set the molecular weights and atomic numbers to 38 and 19, respectively, and the thickness of the material to 1 cm for all six materials to facilitate comparison between the charging cases.

3 - BULK CHARGING EXAMPLES

Electric fields and charge densities as a function of depth and the maximum electric fields anywhere in the material as a function of time are presented in this section for a variety of orbits. Geostationary orbit is treated first to provide a comparison with the results from the CRRES spacecraft followed by lunar transit trajectory. In each case, the orbits are treated for inclinations of 0 degrees, 30 degrees, and 60 degrees from the Earth equator to examine the effect of sampling the Earth's radiation belts over a range of inclinations.

Electron flux as a function of energy is obtained from the AE-8 solar maximum model at 30 energies from 0.04 MeV to 7 MeV at 60 second time steps. Since the transport algorithms used in the NUMIT code are limited to energies in the range of $0.100 \text{ MeV} < E < 100 \text{ MeV}$, the first energy channel does not contribute to either dose or charge deposition in the model. In addition, the final 7 MeV energy channel is also neglected. Parameters for radius of the Earth (R_E) and radius of the Moon (R_L) are taken to be 6371 km and 1738 km, respectively, for this study.

3.1 - GEOSTATIONARY TRANSFER ORBIT

Our 250 km ($0.039 R_E$) perigee altitude by 38226 km ($6.0 R_E$) apogee altitude geostationary transfer orbit actually carries the spacecraft to a distance slightly beyond geostationary orbit altitude ($5.6 R_E$ altitude). This orbit is comparable to the 350 km altitude x 33584 km altitude x 18.1 degree

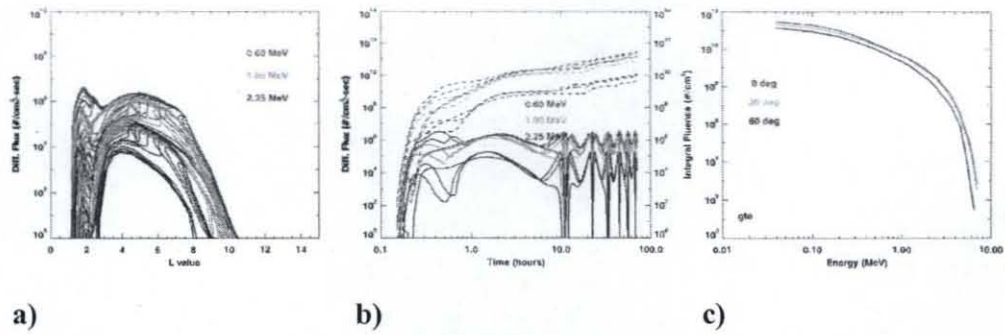


Figure 2. GTO Environment. (a) Integral electron flux as function of L-value, (b) integral electron flux as function of time along orbit, and (c) integral electron fluence for the complete three day period.

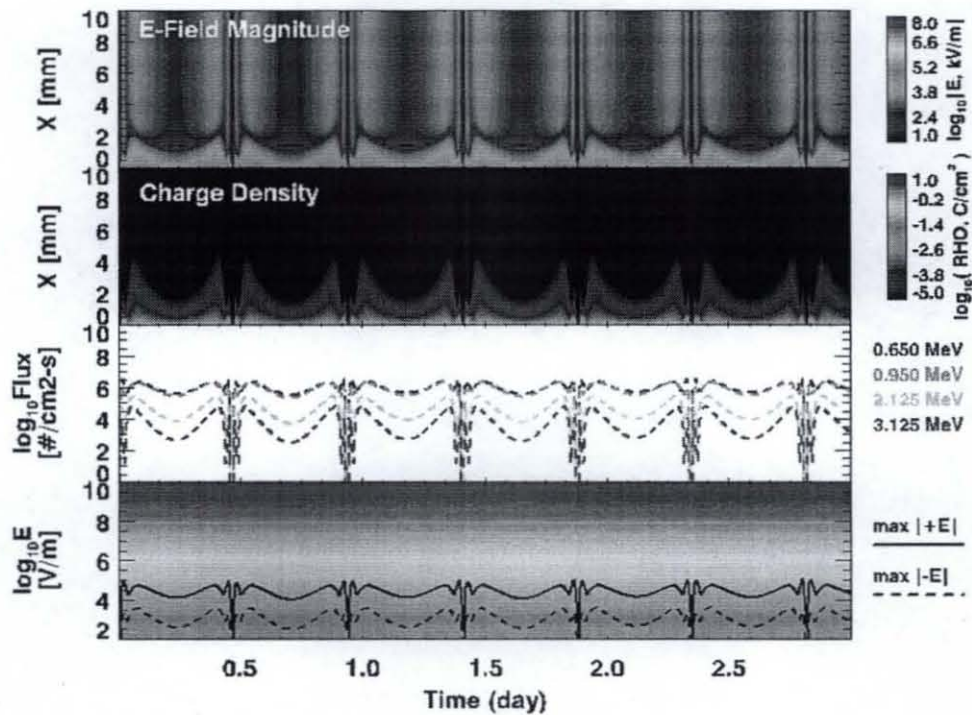


Figure 3. GTO (0 deg) Charging Results, Material 1. Electric field magnitude and charge density are shown in the top two panels and electron flux at four energies are shown in the first panel from the bottom. The maximum positive and negative electric field values are shown in the bottom panel with a color scheme to indicate a relative level of threat for electrostatic discharge.

inclination orbit of the CRRES spacecraft. The orbit ephemeris is computed for a period of three days which provides a number of samples through the radiation belts with an orbital period of 11.3 hours.

Electron environments along the orbit are given in Figure 2. Electron integral flux at three energies as a function of McIlwain's L-value is shown in Figure 2-a. In addition, each energy includes three separate lines indicating the electron integral flux along the 0, 30, and 60 degree inclination orbit (with the greatest flux at 0 degree and the least at 60 degree). Figure 2-b shows the variation in electron integral flux (solid line) and electron integral fluence (dotted line) as a function of time along the spacecraft trajectory. Electron integral fluence accumulated during the complete three day period is shown in Figure 2-c for each of the three orbital inclinations. The AE-

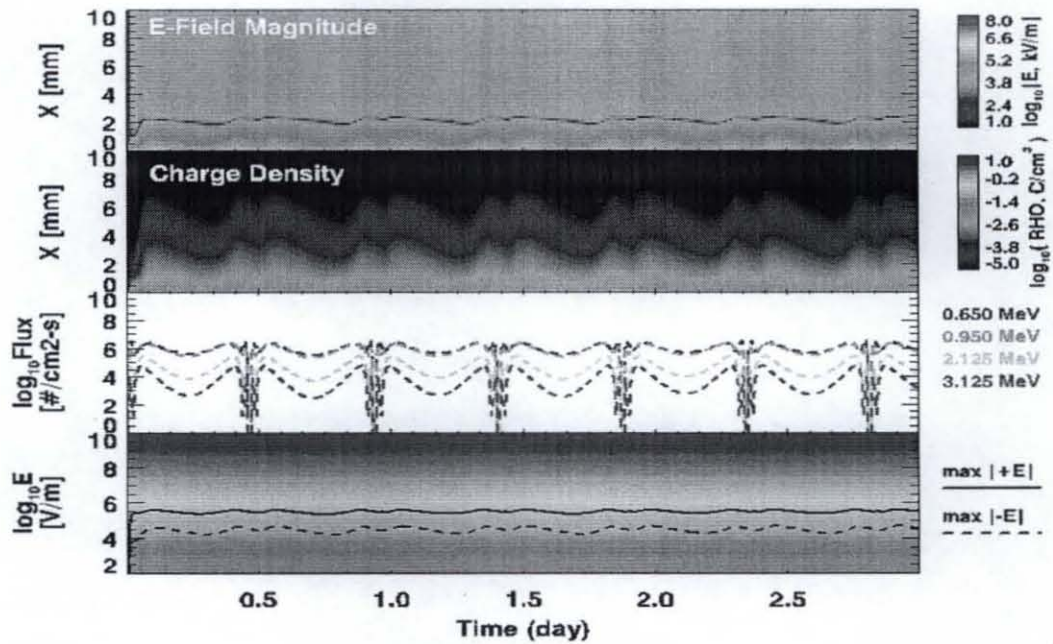


Figure 4. GTO (0 deg) Charging Results, Material 2. The format is given in Figure 3.

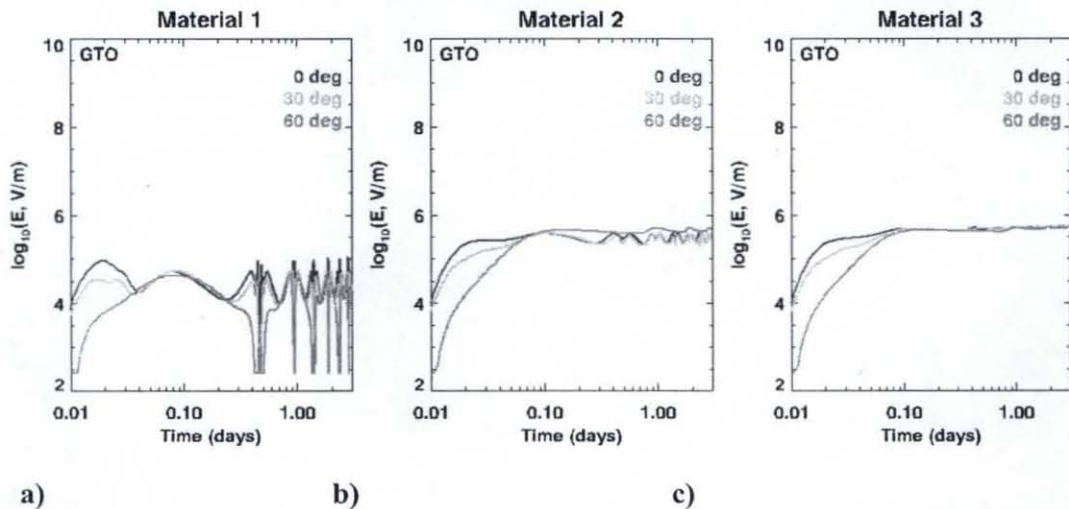


Figure 5. GTO Electric Field Summary. Maximum electric field in (a) Material 1, (b) Material 2, and (c) Material 3 are shown for 0 degree, 30 degree, and 60 degree inclination GTO orbits.

8 solar maximum model provides the electron flux environment so the results are for a mean solar maximum condition within the Earth's radiation belts.

Output from the NUMIT model for the 0 degree inclination case using Material 1 is shown in Figure 3. The top panel presents the simulation time on the horizontal axis, the depth in the material on the vertical axis, and the magnitude of the electric field indicated by the color table. The next panel from the top is the charge density presented in a similar format to the electric field magnitude. The maximum positive and negative electric fields at each time step in the material are plotted in the bottom panel. The background color scheme indicates the relative threat to ESD due to accumulation of charge since many dielectrics exhibit breakdown strengths on the order of 10^7 to

10^8 V/m [4002 Hand book, Shugg, 1986]. However, we emphasize that the color coding is only meant to provide a guide since breakdown strength depends on many factors including material thickness, exposure duration to high electric field conditions, and temperature [Minow and Parker, 2007]. Electron flux at four representative energies is given in the first panel from the bottom to show correlations between the NUMIT output and the input electron environments.

Electric fields and charge densities are moderate in the case where Material 1 is exposed to the 0 degree inclination GTO environment. The relative large 1×10^{-15} S/m dark conductivity allows charge to conduct from the sample when the electron flux is low and reduces the charge density during encounters with the high flux environments in the inner and outer electron radiation belts. Maximum electric fields are only on the order of 10^5 V/m suggesting little threat to breakdown.

Figure 4 presents NUMIT output for Material 2 in the same 0 degree inclination GTO environment. Charging increases due to the increased electron retention by the less conductive Material 2 and the 2.5 hour charging time constant allows the charge density to persist when the vehicle leaves the high flux regions of the orbit compared to the rapid drop in charge density for Material 1 with the 265 second charging time constant.

A summary of maximum electric field magnitudes for Material 1, 2, and 3 generated over a three day period in the GTO orbit are shown in Figure 5. The horizontal axis is time in a logarithmic format to allow detailed examination of the electric fields generated during the initial encounters with the radiation belts while the compressed time one day and beyond exhibit the electric field general trends. All three materials exhibit stronger charging during the initial encounter with the inner radiation belt but evolve to nearly the same electric field in the outer radiation belt. Because the $\tau \sim 265$ second charging time constant for Material 1 is much shorter than the orbital period (11.3 hours) and the time between the inner and outer electron belts, the electric field magnitudes in Figure 5-a follow the same trend as the electron flux along the orbit. Electric field magnitudes continue to exhibit modulation over the full three day simulation period because the short time constant leads to rapid approach to equilibrium charge density and electric field values. In addition, the charging decreases with increasing orbit inclination within the inner radiation belts but are nearly the same in the outer radiation belt. Maximum electric fields are less than $\sim 10^5$ V/m indicating little threat for ESD in any of the inclinations.

Material 2 results shown in Figure 5-b exhibit some modulation of the electric field magnitude along the orbit since the Material 2 charging constant of $\tau \sim 2.5$ hours is less than the 11.3 hour orbital period. However, the inner and outer belts are sampled twice per orbit with a period of a few hours between the peak electron flux within each belt so there is sufficient integration of charge density without the possibility of loss through conduction that the electric field magnitude is greater than Material 1 and the modulation is less than an order of magnitude compared to the one to two order of magnitude modulation exhibited by Material 1. The maximum electric field magnitude in Material 2 after three days is on the order of $\sim 3 \times 10^5$ V/m, greater than Material 1 but still less than typical breakdown strengths for most dielectric materials.

Electric field magnitudes for Material 3 shown in Figure 5-c continue to increase over the full three day simulation period. The charging time constant for Material 3 is $\tau \sim 31$ days, longer than the 11.3 hour orbital period so the material integrates charge over the complete orbit during exposure to the radiation belts. The maximum electric fields in Material 3 for all three orbital inclinations is $\sim 6 \times 10^5$ V/m. Even though the 1×10^{-19} S/m dark conductivity of Material 3 is relatively small, the electron flux provided by the AE-8 solar maximum model is insufficient to produce electric fields in the material which exceed electric fields of $\sim 10^7$ V/m where the onset of dielectric breakdown begins to occur.

3.2 – EARTH-MOON TRANSFER ORBIT

Direct co-planar transfer orbits from the Earth to the Moon are only possible when the translunar/trans-Earth injection orbit lies in the plane of the Moon's orbit. The inclination of the lunar orbit varies from 18.2 to 28.5 degrees relative to the Earth's equator with a period of 18.6 years. Direct orbits originating from due east launches are possible only from launch sites at latitudes ≥ 28.5 degrees latitude and other sites must generally use non-coplanar trajectories. For example, co-planar trajectories are possible from Kennedy Space Center at 28.5 degrees north latitude once every 18.6 years but higher inclination orbits must be used at other times.

The ten Apollo program flights which orbited the Moon (Apollo 8 through Apollo 17) all were launched from what is now the Kennedy Space Center (KSC) on the east coast of Florida at 28.5 degree north latitude. A direct ~ 28.5 degree inclination coplanar translunar injection orbit was only possible from KSC during the Apollo era on 25 March 1969 when the Moon was at an extreme north declination of $28^{\circ}43'32''$ and additional dates [Meeus, 1997] when the coplanar trajectories are possible from KSC include 15 September 1987 ($28^{\circ}42'52''$), 15 September 2006 ($28^{\circ}43'22''$), 7 March 2025 ($28^{\circ}43'00''$), and 25 September 2043 ($28^{\circ}43'109''$). All other times the flight inclination will be greater than the minimum inclination obtained from a due east launch resulting in reduced radiation dose. Translunar injection orbit inclinations utilized for the Apollo flights ranged from a minimum of 28.5 degrees to a maximum of 32.55 degrees [Orloff, 2000]. More recently, the Lunar Prospector spacecraft (also launched from 28.5 degrees north latitude at Cape Canaveral Air Force Station) utilized a 29.2 degree inclination translunar injection orbit [Lozier *et al.*, 1998]. In contrast, the Clementine spacecraft was launched from Vandenberg Air Force Base at 34.75 deg north latitude into a lunar injection orbit inclined at 67 degrees [Regeon *et al.*, 1994] and the European Space Agency Smart-1 spacecraft launched from the near-equatorial 5.05 deg north latitude facility at Kourou, French Guiana, utilized a translunar injection orbit initially inclined 7 degrees from the equator [ESA, 2003]. Finally, the series of Russian Luna probes launched in the 1960's and 1970's from Baikanur, Khazakstan, into near polar orbits with inclinations of 73 deg received some of the smallest radiation doses while traversing Earth's radiation belts.

We simulate the Earth-Moon transfer orbit by adopting an elliptical orbit with perigee altitude of 250 km and apogee altitude of 379,867 km required for a 100 km lunar orbit insertion altitude on the far side of the Moon from the Earth. Apogee altitude is obtained by considering the mean distance between the center of the Earth and the center of the Moon is 384,400 km, the radius of the Earth is 6371 km, and the radius of the Moon is 1738 km. The period of the orbit is approximately 10 days yielding a transit time to the Moon of approximately 5 days. Orbit inclinations of 0 degrees, 30 degrees, and 60 degrees are considered here.

Electron environments along the orbit are given in Figure 6 with electron integral flux at three energies as a function of McIlwain's L-value in Figure 6-a, electron integral flux (solid lines) and electron integral fluence (dotted line) as a function of time along the transfer orbit in Figure 6-b, and the accumulated electron integral fluence accumulated during the complete three day simulation period in Figure 6-c. Note that the simulation period is only three days while the time required to reach the Moon is ~ 5 days which is acceptable because the AE-8 model does not provide electron flux beyond 11 R_E , a distance the spacecraft passes within four or five hours after the trans-lunar insertion burn at perigee places the vehicle on the trajectory towards the Moon. The AE-8 solar maximum values are used for the environments in this case.

NUMIT output for exposure of Material 1 to the electron environments along the 30 degree inclination Earth-Moon transfer orbit is shown Figure 7. The charging time constant of $\tau \sim 265$ seconds is much less than the four to five hours required to transit the radiation belts so the electric field magnitude generated within the material quickly rise to a maximum value of less than 10^5 V/m during transit of the radiation belts and quickly return to a background once the vehicle has left the trapped radiation environment. In comparison, Figure 8 provides NUMIT output Material 2 along

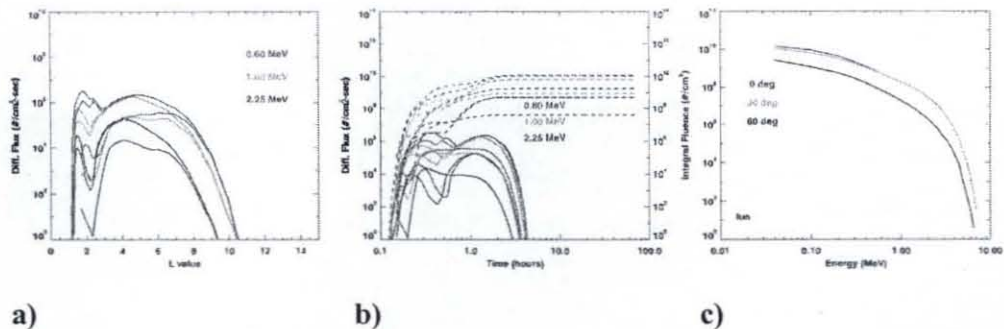


Figure 6. Earth-Moon Lunar Transit Environment. (a) Integral electron flux as function of L-value, (b) integral electron flux as function of time along orbit, and (c) integral electron fluence for the complete three day period.

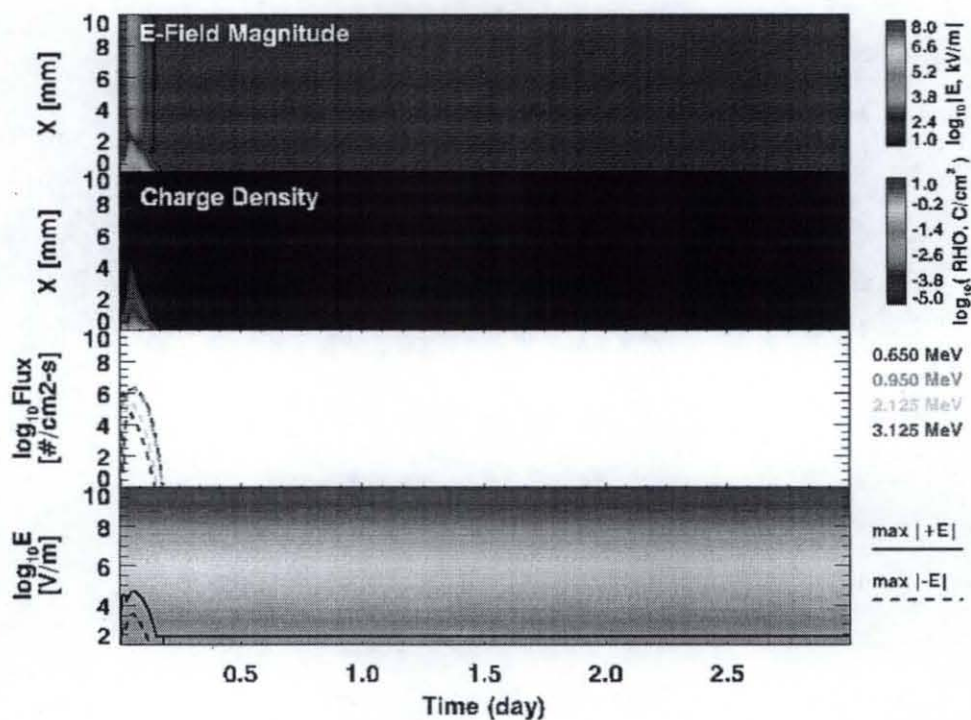


Figure 7. Earth-Moon (30 degree) Lunar Transit Environment, Material 1. The format is given in figure 3.

the same orbit and environment. The $\tau \sim 2.5$ hours charging time constant for Material 2 is on the same order of magnitude as the four to five hour transit time of the radiation belts so the maximum electric field magnitude within the belts increases to values approaching 3×10^5 V/m and nearly three quarters of a day is required for the field to decrease to the background after leaving the radiation belts.

Figure 9 is the summary of maximum electric field magnitudes for Materials 1, 2, and 3 generated over the first three days of the five day Earth-Moon transfer orbit including the time from departure from low Earth orbit and transit of the radiation belts. Electric field magnitudes increase as the conductivity of the materials decrease but the worst case charging conditions still only produce maximum electric field magnitudes of $\sim 4 \times 10^5$ V/m in the low conductivity Material 3.

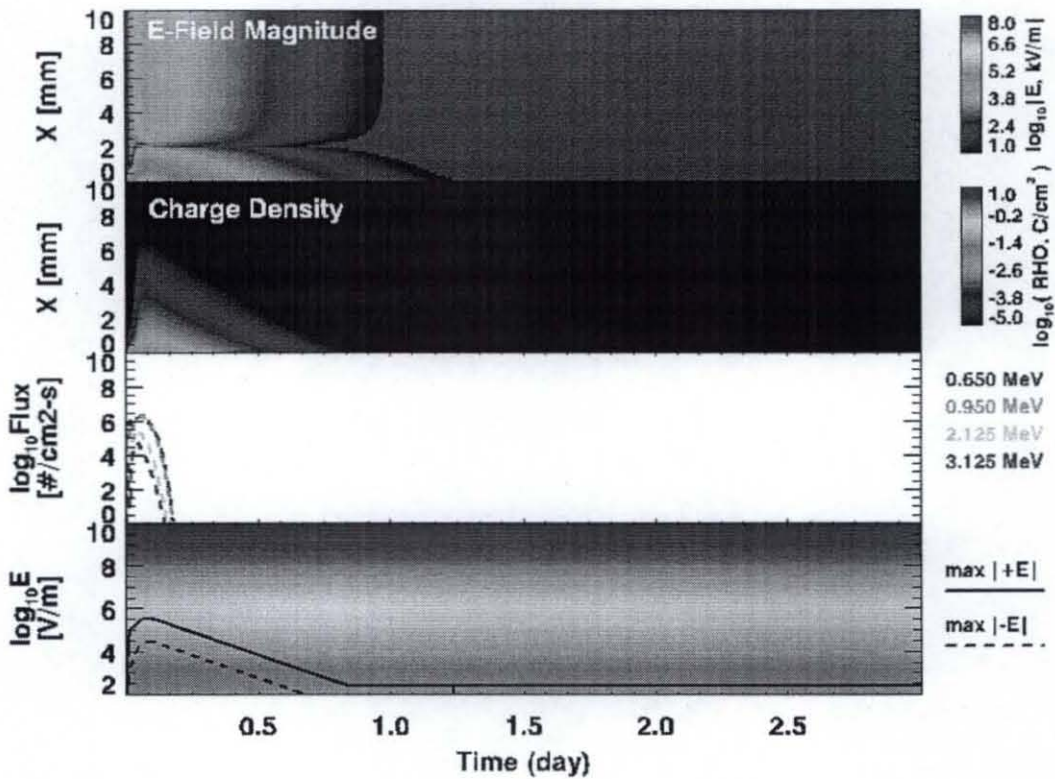


Figure 8. Earth-Moon (30 degree) Lunar Transit Environment., Material 2. The format is given in figure 3.

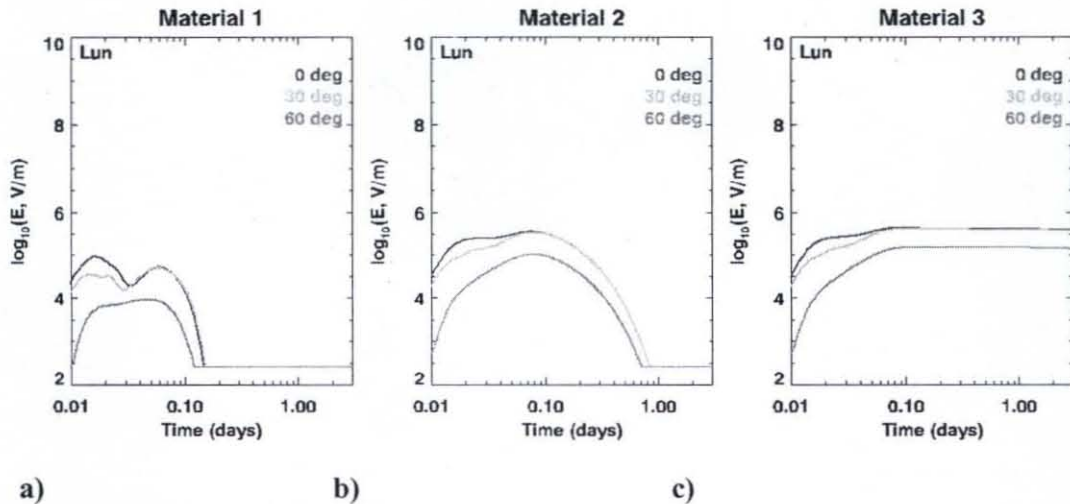


Figure 9. Lunar Transit Electric Field Summary. Maximum electric field in (a) Material 1, (b) Material 2, and (c) Material 3 are shown for 0 degree, 30 degree, and 60 degree inclination lunar transfer orbits.

3.3 – EXTREME ENVIRONMENT DURING LUNAR TRANSIT

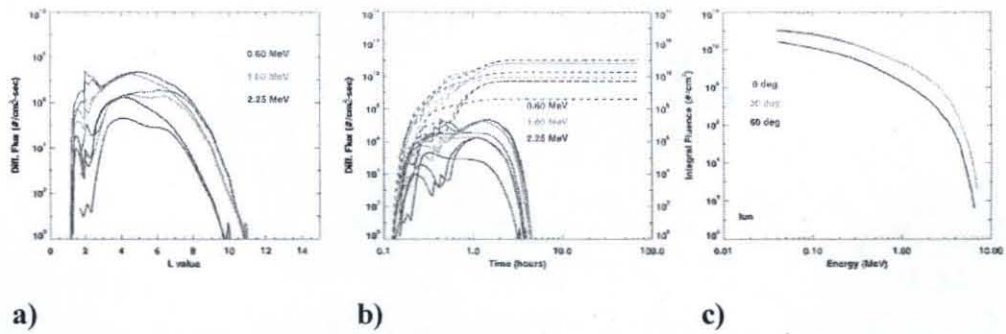


Figure 10. Extreme Earth-Moon Lunar Transit Environment. (a) Integral electron flux as function of L-value, (b) integral electron flux as function of time along orbit, and (c) integral electron fluence for the complete three day period.

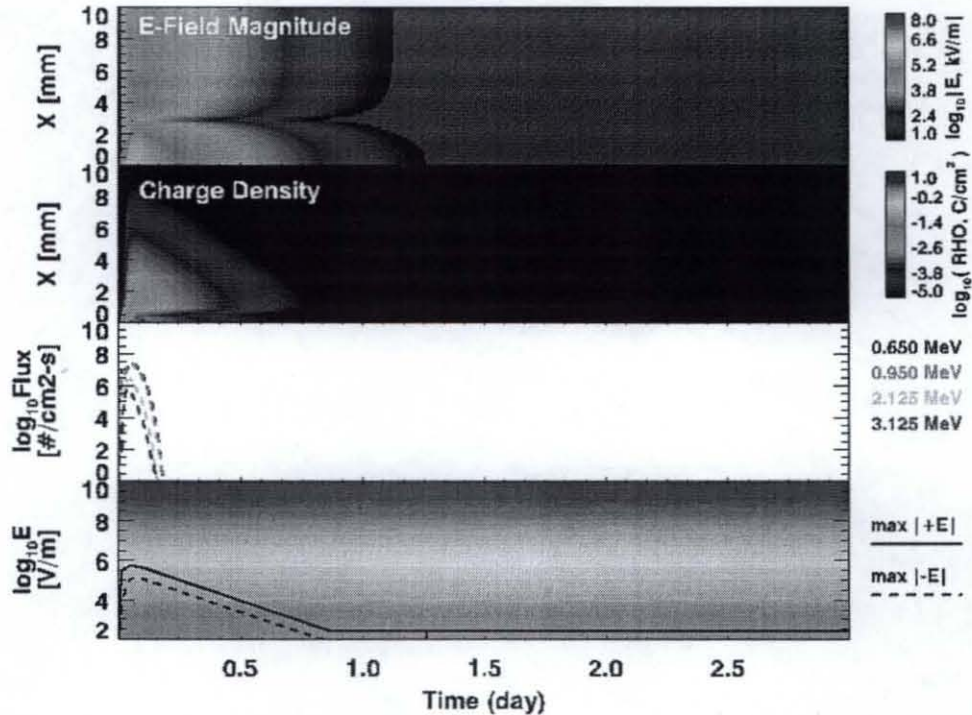


Figure 11. Earth-Moon (30 degree) Lunar Transit in Extreme Environment, Material 2. The format is given in figure 3.

The examples shown in the previous two sections only considered the mean AE-8 electron environment for each of the spacecraft trajectories. However, it is known that the electron flux in the outer radiation belts may be enhanced by an order of magnitude or two during geomagnetic storms or when the magnetosphere strongly interacts with high speed solar wind streams. We consider extreme electron flux environments here by arbitrarily multiplying the AE-8 electron flux at all energies by a factor of 10x for L-values greater than or equal to L=2. The effect is to increase the flux in the electron slot and outer radiation belts while preserving the mean AE-8 flux in the inner electron belt. The approximation is valid because the source of the inner electron radiation belt is the decay of albedo neutrons generated by nuclear interactions of cosmic rays with the Earth's atmosphere and the inner belt does not exhibit the large variations in electron flux observed in the outer electron belt. Figure 10 provides the environment summary panels for the extreme solar maximum environments that will be used in the following examples.

NUMIT output for Material 2 is given in Figure 11 for a 30 degree inclination Earth-Moon transfer orbit through the extreme environment. Electric field magnitudes approach 10⁶ V/m during transit

of the radiation belts, an order of magnitude below the $\sim 10^7$ V/m threshold for the onset of arcing. However, as a warning that these results do not indicate safe passage to lunar destinations for all materials through the radiation belts, we show NUMIT results in Figure 12 for Material 4 indicating strong electric field development exceeding the $\sim 10^7$ V/m threshold and even the $\sim 10^8$ V/m fields at which many dielectrics are known to break down. Material 4 is representative of an epoxy-fiberglass material for which the electrical properties have been measured in the laboratory [Rodgers et al., 2003]. Material 4 is a particular threat to bulk charging because of the relatively low 2.19×10^{-18} S/m dark conductivity and the “negligible” radiation induced conductivity. It is unlikely Material 4 would actually sustain the large electric fields resulting from the NUMIT model but dielectric failure is not currently included in the code.

As final example, we demonstrate the effect of temperature on electric field development within the dielectric. The 1×10^{-15} S/m dark conductivity and $k_p = 1 \times 10^{-18}$ S/m-rad-s⁻¹ radiation induced conductivity constant for Material 5 represent the electrical properties of a dielectric material at room temperature and Material 6 is the same material at a cryogenic temperature of ~ 100 K. Decreasing the temperature of materials to cryogenic temperatures has been shown to decrease the dark conductivity by two to three orders of magnitude with little change in the dielectric constant [c.f, Minow and Parker, 2007]. Exposure of a 1 cm thick sample of Material 5 to the extreme 30 degree inclination lunar transit environment gives a maximum electric field of 5.71×10^5 V/m which occurs 1.48 hours after perigee during radiation belt transit. After leaving the radiation belts the electric field quickly decreases since the material conductivity is sufficient to allow the accumulated charge to conduct out of the charged dielectric material. The situation at ~ 100 K shown in Figure 13 is quite different. The maximum electric field is 1.05×10^7 V/m which occurs 3.25 hours after perigee and the subsequent decay of the charge density following exposure to the radiation belts results in a maximum electric field magnitude of 0.41×10^7 V/m at the end of the three day period. While the electric field generated by the space radiation environment is well below the $\sim 10^7$ V/m breakdown strength of many dielectric materials at ambient temperatures, the same dielectric exhibits a field sufficient to suggest a threat of ESD at ~ 100 K.

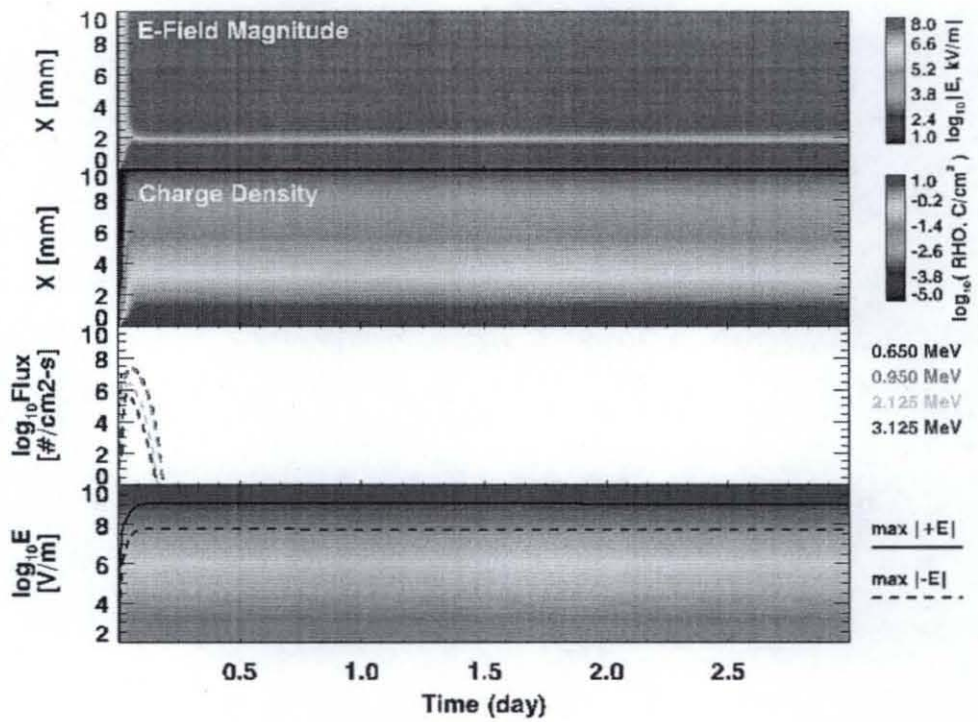


Figure 12. Earth-Moon (30 degree) Lunar Transit in Extreme Environment., Material 4. The format is given in figure 3.

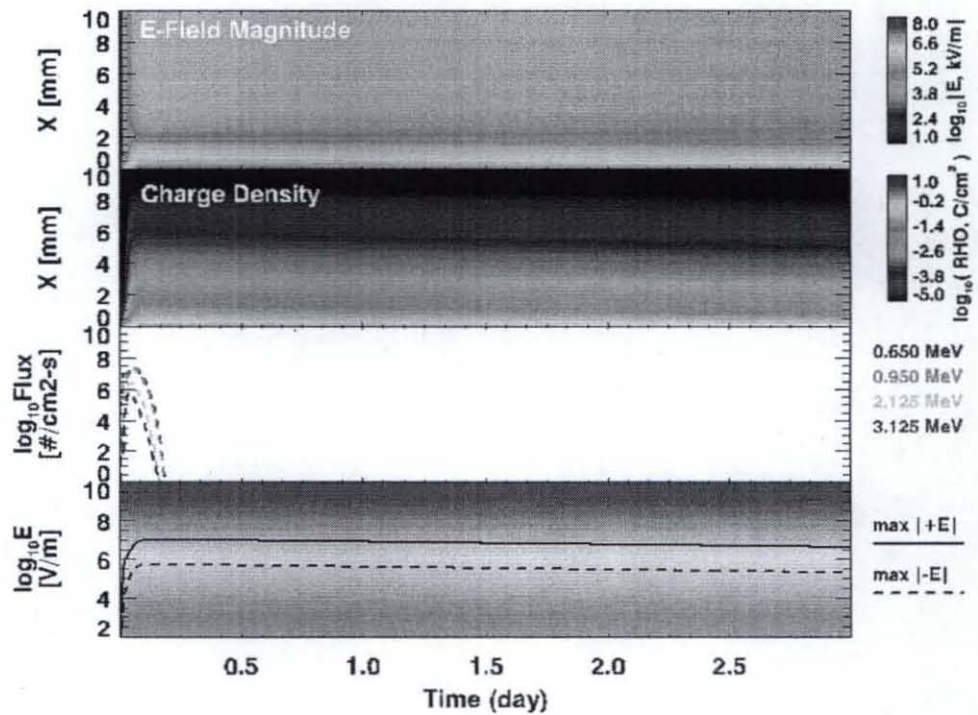


Figure 13. Earth-Moon (30 degree) Lunar Transit in Extreme Environment., Material 6. The format is given in figure 3.

Modification of the NUMIT 1-D bulk charging model to read tables of electron flux energy spectra as a function of time along a spacecraft trajectory provides a convenient method for screening dielectric materials for potential ESD risk. Results presented here show the NUMIT output provides electric field values consistent with those reported in the literature for multiple passes through the Earth's radiation belts on GTO orbits. In addition, we have demonstrated that exposure of dielectric materials to bulk charging environments on Earth-Moon transfer orbits can result in development of electric fields which approach or even exceed the dielectric breakdown strength of dielectric materials. Measurement of electrical properties of dielectric materials and careful evaluation of dielectric materials for use in future lunar programs will be required to assure successful operations during transit of the radiation belts.

5 - ACKNOWLEDGEMENTS

The NUMIT model was originally developed by Dr. A.R. Frederickson and provided to MSFC by his colleagues at JPL. Contributions by IJ and HBG were carried out at the Jet Propulsion Laboratory, California Institute of Technology, under a contract with the National Aeronautics and Space Administration.

6 - BIBLIOGRAPHY

- Armstrong, T.W., and B.L. Colborn, Evaluation of Trapped Radiation Model Uncertainties for Spacecraft Design, NASA CR-2000-210072, March, 2000.
- Avoiding problems caused by spacecraft on-orbit internal charging effects, *NASA-HDBK-4002*, 2004.
- Daly, E.J., P. Buhler, and M. Kruglanski, Observations of the outer radiation belt with REM and comparisons with models, *IEEE Trans. Nuc. Sci.*, 46, 1469 – 1474, 1999.
- Daly, E.J., J. Lemaire, D. Heynderickx, and D.J. Rodgers, Problems with models of the radiation belts, *IEEE Trans. Nuc. Sci.*, 43, 403 – 415, 1996.
- ESA 2003, SMART-1 leaves Earth on a long journey to the Moon, ESA Press Release Number 60-2003, 28 September 2003, available at:
http://nssdc.gsfc.nasa.gov/planetary/text/smart1_pr_20030928.txt
- Frederickson, A.R., Radiation Induced Electrical Current and Voltage in Dielectric Structures, AFRL-TR-74-05823, 1974.
- Frederickson, A.R., Radiation induced currents and conductivity in dielectrics, *IEEE Trans. Nuc. Sci.*, NS24, 2532 – 2539, 1977.
- Frederickson, A.R., Radiation induced dielectric charging, in "Space Systems and Their Interactions with Earth's Space Environment, Vol. 71, Progress in Astronautics and Aeronautics, H.B. Garrett and C.P. Pike (eds.), AIAA, p. 386 – 412, 1980.
- Frederickson, A.R., Electric Discharge Pulses in Irradiated Solid Dielectrics in Space, *IEEE Transactions on Electrical Insulation* Vol. 18, pp. 337-349, 1983.
- Frederickson, A.R., *et al.*, "Radiation-induced insulator pulses in the CRRES internal discharge monitor satellite experiment," *IEEE Trans. Nucl. Sci.*, vol. 38, p. 1614, Dec. 1991.
- Frederickson, A.R., *et al.*, "Characteristics of spontaneous electrical discharging of various insulators in space radiations," *IEEE Trans. Nucl. Sci.*, vol. 39, p. 1773, Dec. 1992.

- Frederickson, A.R., "Methods for estimating spontaneous pulse rates for insulators inside spacecraft," *IEEE Trans. Nucl. Sci.*, vol. 43, p. 2778, Dec. 1996.
- Frederickson, A.R., and J.T. Bell, Analytic approximation for charge current and deposition by 0.1 to 100 MeV electrons in thick slabs, *IEEE Trans. Nuc. Sci.*, 42, 1910, 1995.
- Fredrickson, A.R., and D.H. Brautigam, Mining CRRES IDM Pulse and CRRES Environmental Data to Improve Spacecraft Charging/Discharging Models and Guidelines, NASA CR 2004-213228, June, 2004.
- Halekas, J.S., R.P. Lin, and D.L. Mitchell, Large negative lunar surface potentials in sunlight and shadow, *Geophys. Res. Lett.*, 32, 9102, 2005.
- Halekas, J.S., G.T. Delory, D.A. Brain, R.P. Lin, M.O. Fillingim, C.O. Lee, R.A. Mewaldt, T.J. Stubbs, W.M. Farrell, and M.K. Hudson, Extreme lunar surface charging during solar energetic particle events, *Geophys. Res., Lett.*, 34, 2111, 2007.
- Jun, I., H.B. Garrett, W. Kim, and J. Minow, Review of an internal charging code, NUMIT, to be presented at the 10th International Spacecraft Charging Conference, Biarritz, France, June 18-21 June, 2007.
- Kawakita, S., H. Kusawake, M. Takahashi, H. Maejima, T. Kurosaki, Y. Kojima, D. Goto, Y. Kimoto, J. Ishizawa, M. Nakamura, J-H Kim, S. Hosoda, M. Cho, K. Toyoda, and Y. Nozaki, Investigation of an Operational Anomaly of the ADEOS-II Satellite, 9th Spacecraft Charging Technology Conference, JAXA-SP-05-001E, Tsukuba, Japan, 2005.
- Lauenstein, J-M., and J.L. Barth, Radiation belt modeling for spacecraft design: Model comparisons for common orbits, *IEEE Radiation Effects Data Workshop*, 2005.
- Lozier, D., K. Galal, D. Folta, and M. Beckman, Lunar Prospector mission design and trajectory support, AAS Paper 98-323, 1998.
- Minow, J.I., and L.N. Parker, Spacecraft Charging in Low Temperature Environments, AIAA-2007-1095, 45th AIAA Aerospace Sciences Meeting, Reno, NV, 8-11 January 2007.
- Meeus, J., *Mathematical Astronomy Morsels*, Willmann-Bell, Inc., Richmond, Virginia, 1997.
- Orloff, R.W., *Apollo by the Numbers: A Statistical Reference*, NASA SP-2000-4029, NASA Headquarters, Washington, DC, 2000.
- Purvis, C.K., H.B. Garrett, A.C. Whittlesey, and N.J. Stevens, Design guidelines for assessing and controlling spacecraft charging effects, NASA TP-2361, NASA, 1984.
- Regeon, P.A., R.J. Chapman, and R. Baugh, Clementine, "The deep space program science experiment," Paper IAA-L-0501, presented at the International Academy of Astronautics (IAA) International Conference On Low-Cost Planetary Missions, Johns Hopkins University, Applied Physics Laboratory, Laurel, Maryland, 12-15 April 1994.
- Rodgers, D.J., K.A. Ryden, G.L. Wrenn, L. Levy, and J. Sorensen, Fitting of material parameters for DICTAT internal dielectric charging simulations using DCFIT, in *Proc. of the 9th International Symposium on Materials in a Space Environment*, SP-540, Noordwijk, The Netherlands, September, 2003.
- Sessler, G.M., (editor), *Electrets, Topics in Applied Physics, Volume 33, Second Edition*, Springer-Verlag, 1987.
- Sessler et al., Models of charge transport in electron-beam irradiated insulators, *IEEE Transactions on Dielectrics and Electrical Insulation*, 11, 192 – 202, 2004.
- Shugg, W.T., *Handbook of Electrical and Electronic Insulating Materials*, Van Nostrand Reinhold Company, New York, 1986.

Vette, J., The AE-8 trapped electron model environment, National Space Science Data Center, Report 91-24, Greenbelt, Maryland, 1991.

Violet and A. R. Frederickson, "Spacecraft anomalies on the CRRES satellite correlated with the environment and insulator samples," *IEEE Trans. Nucl. Sci.*, vol. 40, p. 1512, 1993.

Wrenn, G.L., Conclusive evidence for internal dielectric charging anomalies on geosynchronous communications spacecraft, *J. Spacecraft and Rockets*, 32, 514 – 520, 1995.

Evaluation of Bulk Charging in Geostationary Transfer Orbit and Earth Escape Trajectories Using the Numit 1-D Charging Model




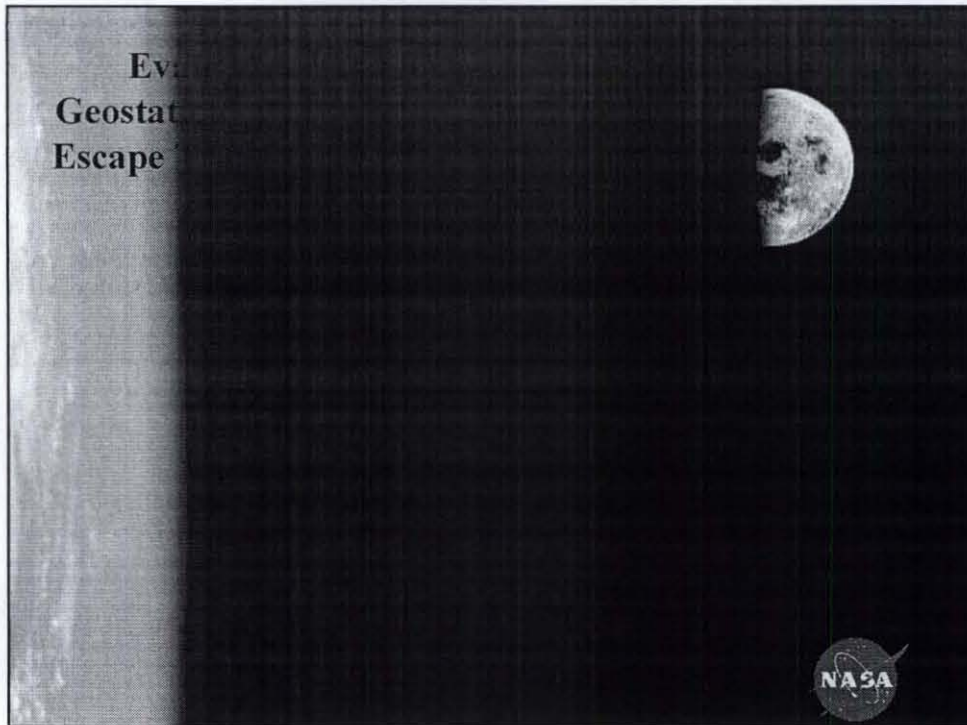
Joseph I. Minow and Victoria N. Coffey
EV13/Natural Environments Branch
NASA, Marshall Space Flight Center

Linda N. Parker and William C. Blackwell, Jr.
Jacobs Engineering, MSFC Group
NASA, Marshall Space Flight Center

Insoo Jun and Henry B. Garrett
The Jet Propulsion Laboratory, The California Institute of Technology

10th Spacecraft Charging Technology Conference
Biarritz, France 18-22 June 2007





Overview

- Introduction
- NUMIT model
- AE-8 Max Examples
 - GTO
 - Lunar transit
 - Deep space escape trajectory
- Worst case example (lunar)
- Summary

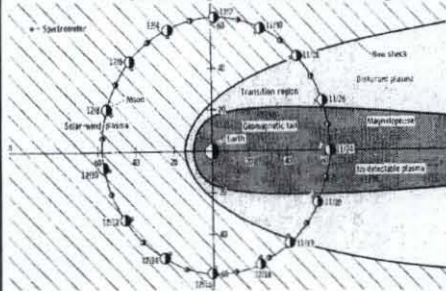
10th SCTC 18-22 June 2007
Biarritz, France

2



Magnetosphere and Lunar Orbit

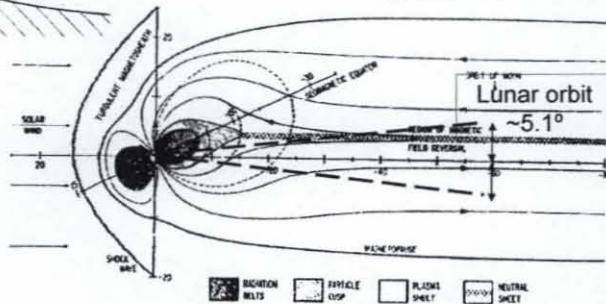
Apollo 12 [NASA SP-235, 1970]



Moon passes through magnetotail and magnetosheath plasma environments every month

Adams et al., 1981

In-situ observations of plasma and radiation environments relevant to lunar exploration are available from pre-Apollo to present



10th SCTC 18-22 June 2007
Biarritz, France

3



Bulk (Deep Dielectric) Charging

- Radiation charging of insulators, isolated conductors

$$\nabla \cdot \mathbf{D} = \rho$$

$$\mathbf{D} = \epsilon \mathbf{E}$$

$$\epsilon = \kappa \epsilon_0$$

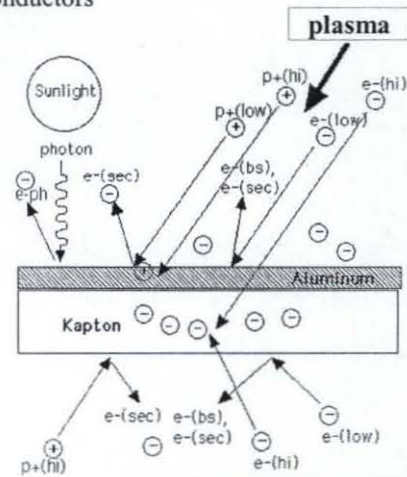
$$\frac{\partial \rho}{\partial t} = -\nabla \cdot \mathbf{J}$$

$$\mathbf{J} = \mathbf{J}_0 + \mathbf{J}_C$$

$$\mathbf{J} = \sigma \mathbf{E}$$

$$= (\sigma_{\text{dark}} + \sigma_{\text{radiation}}) \mathbf{E}$$

$$\sigma_{\text{radiation}} = k \left(\frac{d\gamma}{dt} \right)^\alpha \quad 0.5 < \alpha < 1.0$$



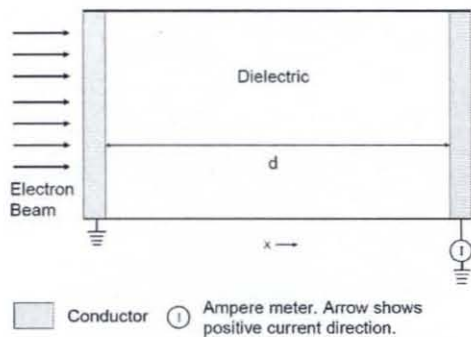
(Garrett and Minow, 2004)

10th SCTC 18-22 June 2007
Biarritz, France

4



NUMIT Geometry



(Jun et al. 2007)

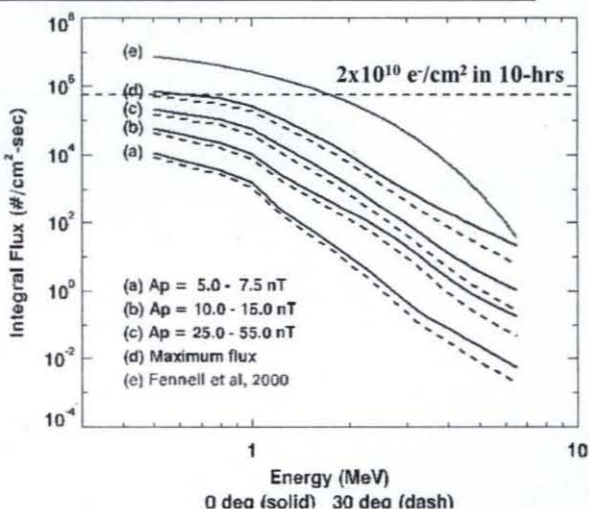
10th SCTC 18-22 June 2007
Biarritz, France

5



Internal (Bulk) Charging

- Translunar and trans-Earth injection trajectories transit the radiation belts
- TLI/TEI orbits are similar to the geostationary transfer orbit environments encountered by CRRES
 - CRRES T~10 hours
10 hours in radiation belt
 - TLI/TEI T~8 days
≤4 hours in radiation belt



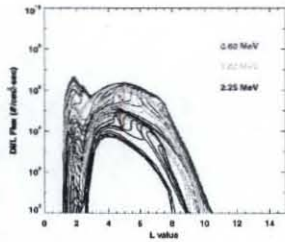
- CRRESELE A_p dependent (a-c), worst case (d) orbit averaged environments
- Fennell et al. 2000 (e) lunar transfer orbit charging environment

10th SCTC 18-22 June 2007
Biarritz, France

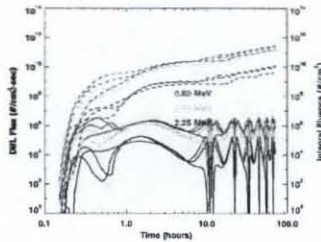
6



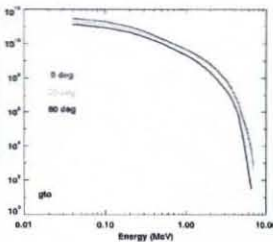
GTO Environments Summary



Flux vs L-value



Flux vs Time



Electron Fluence Spectrum

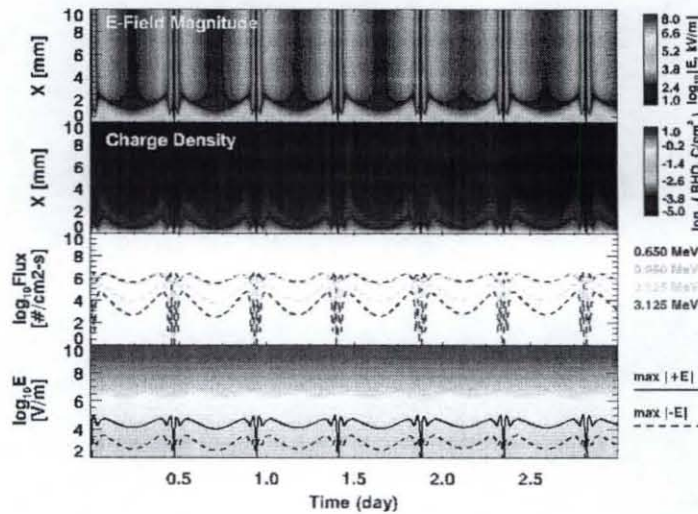
AE-8 solar maximum

10th SCTC 18-22 June 2007
Biarritz, France



GTO

- 0 deg inc
- AE-8 max
- Material 1

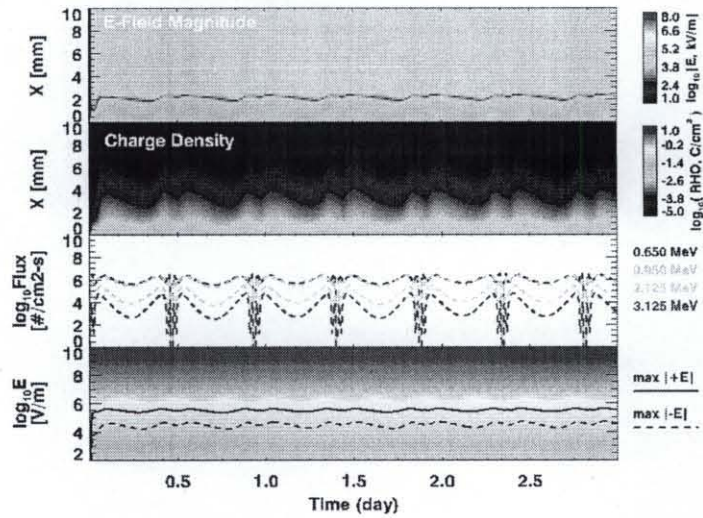


10th SCTC 18-22 June 2007
Biarritz, France



GTO

- 0 deg inc
- AE-8 max
- Material 2

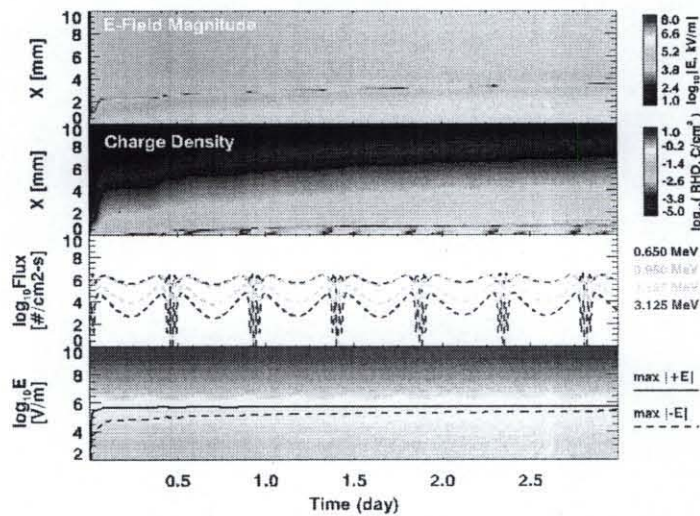


10th SCTC 18-22 June 2007
Biarritz, France



GTO

- 0 deg inc
- AE-8 max
- Material 3

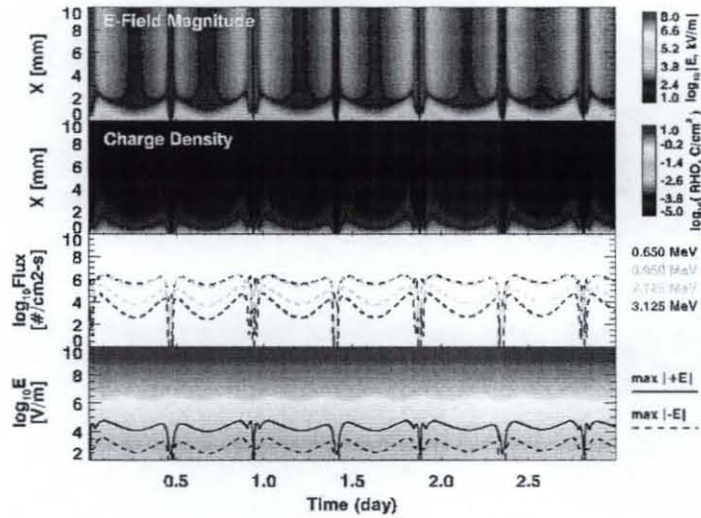


10th SCTC 18-22 June 2007
Biarritz, France



GTO

- 30 deg inc
- AE-8 max
- Material 1



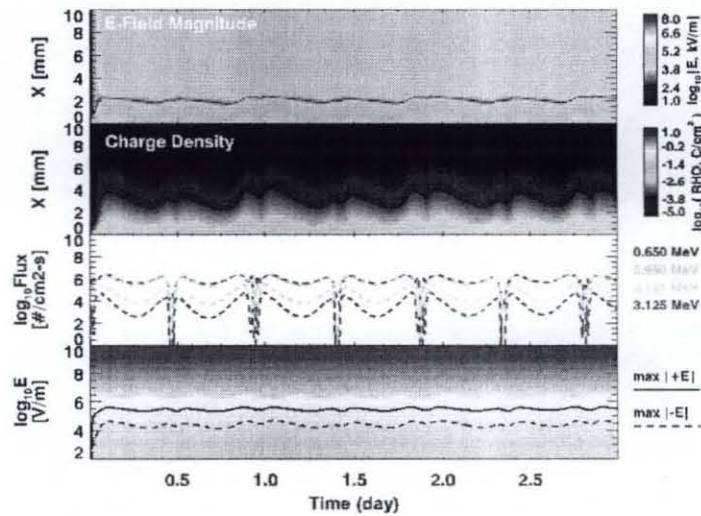
10th SCTC 18-22 June 2007
Biarritz, France

11



GTO

- 30 deg inc
- AE-8 max
- Material 1



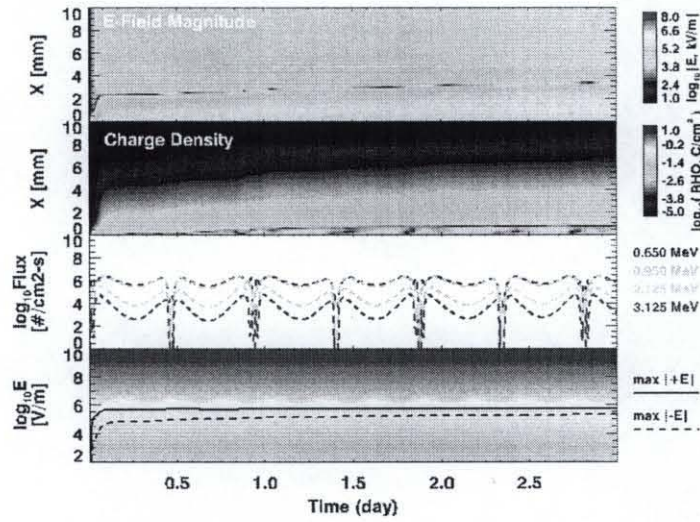
10th SCTC 18-22 June 2007
Biarritz, France

12



GTO

- 30 deg inc
- AE-8 max
- Material 1



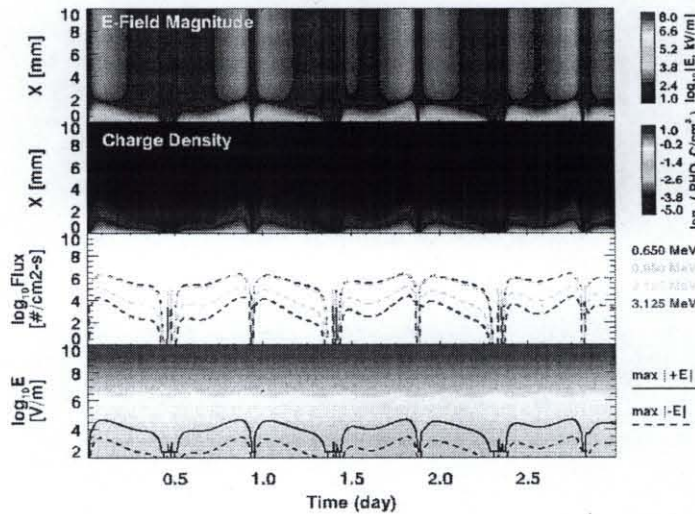
10th SCTC 18-22 June 2007
Biarritz, France

13



GTO

- 60 deg inc
- AE-8 max
- Material 1



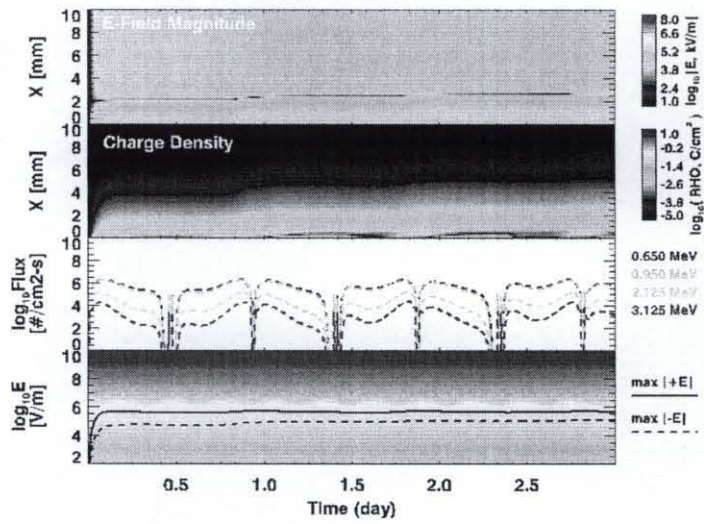
10th SCTC 18-22 June 2007
Biarritz, France

14



GTO

- 60 deg inc
- AE-8 max
- Material 2



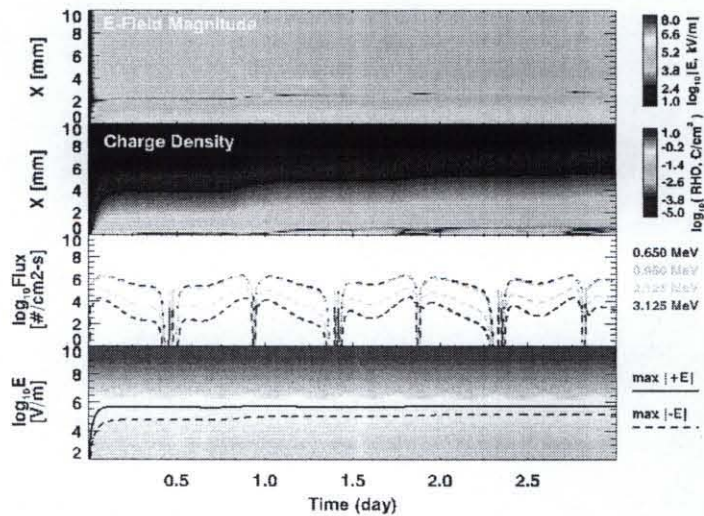
10th SCTC 18-22 June 2007
Biarritz, France

15



GTO

- 60 deg inc
- AE-8 max
- Material 3



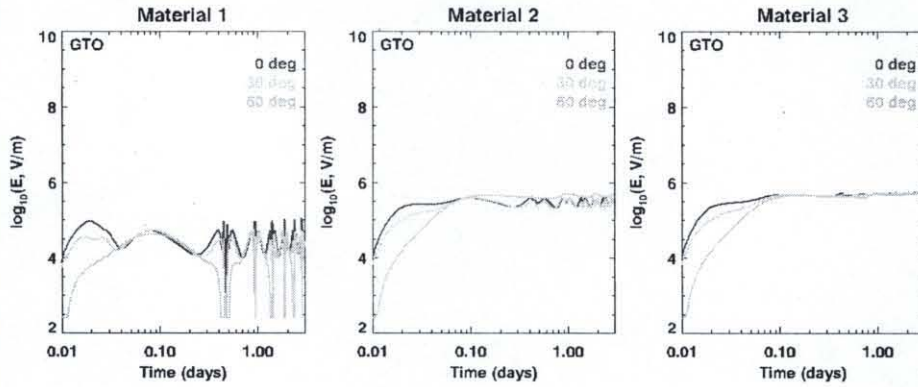
10th SCTC 18-22 June 2007
Biarritz, France

16



GTO Summary

- Maximum electric field

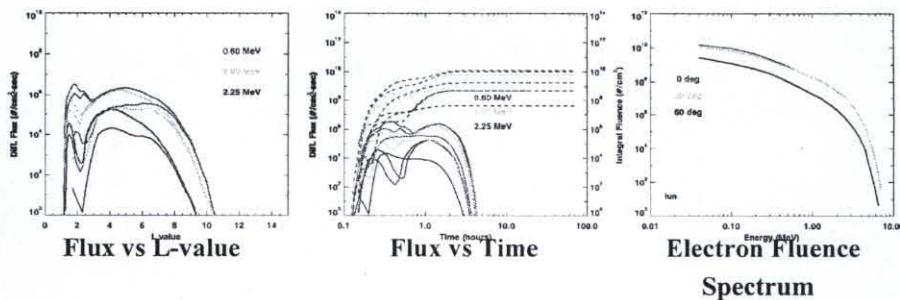


10th SCTC 18-22 June 2007
Biarritz, France

17



Lunar Transit



AE-8 solar maximum

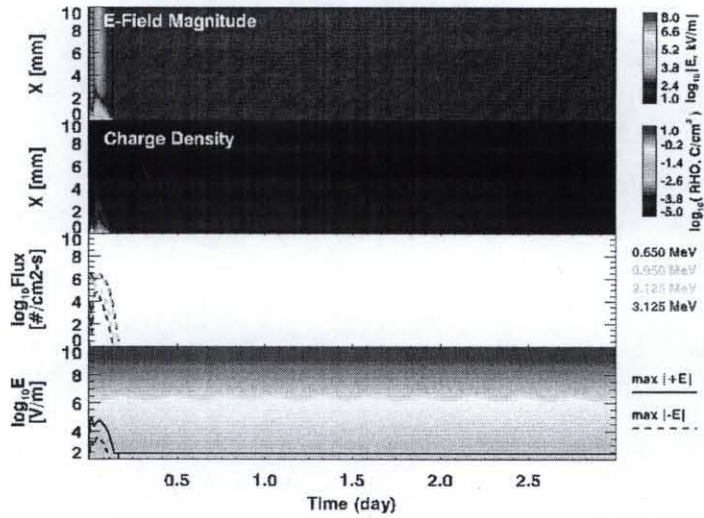
10th SCTC 18-22 June 2007
Biarritz, France

18



Lunar Transit

- 0 deg inc
- AE-8 max
- Material 1

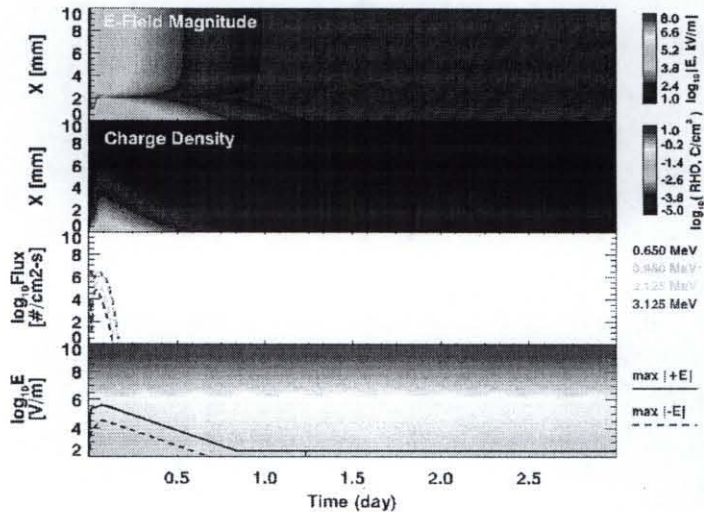


19



Lunar Transit

- 0 deg inc
- AE-8 max
- Material 2

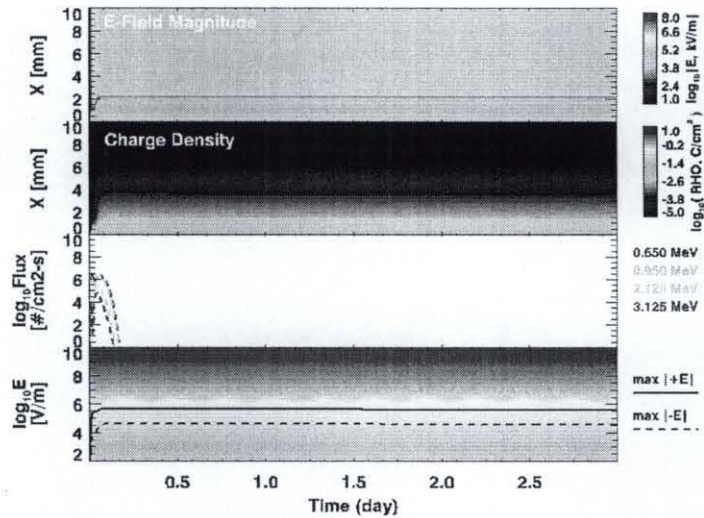


20



Lunar Transit

- 0 deg inc
- AE-8 max
- Material 3



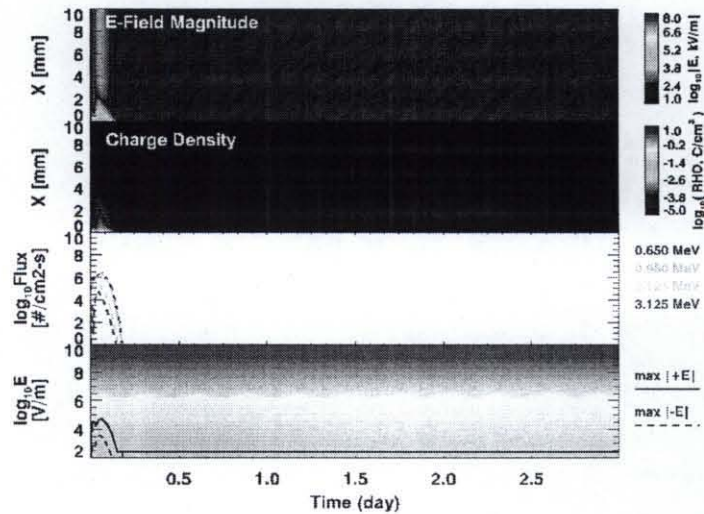
10th SCTC 18-22 June 2007
Biarritz, France

21



Lunar Transit

- 30 deg inc
- AE-8 max
- Material 1



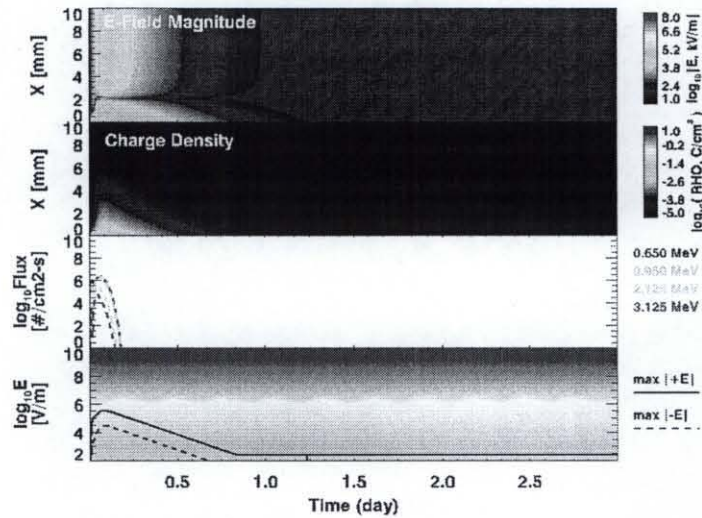
10th SCTC 18-22 June 2007
Biarritz, France

22



Lunar Transit

- 30 deg inc
- AE-8 max
- Material 2



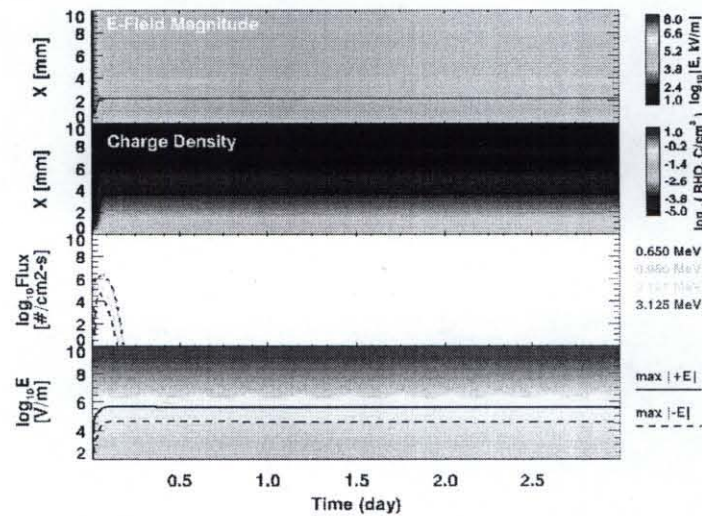
10th SCTC 18-22 June 2007
Biarritz, France

23



Lunar Transit

- 30 deg inc
- AE-8 max
- Material 3



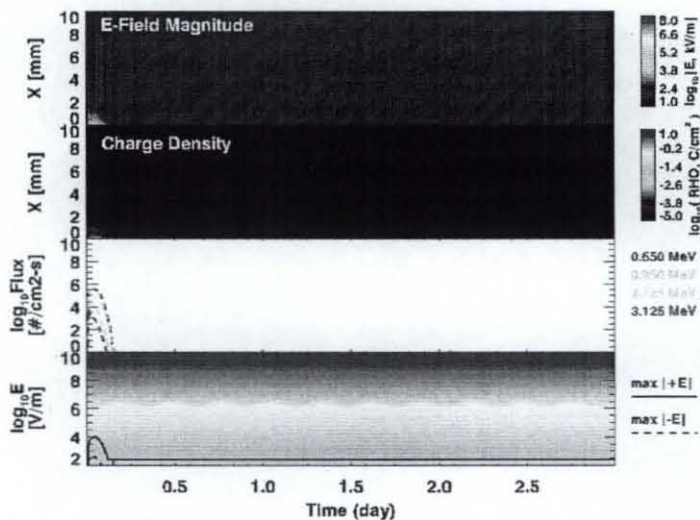
10th SCTC 18-22 June 2007
Biarritz, France

24



Lunar Transit

- 60 deg inc
- AE-8 max
- Material 1



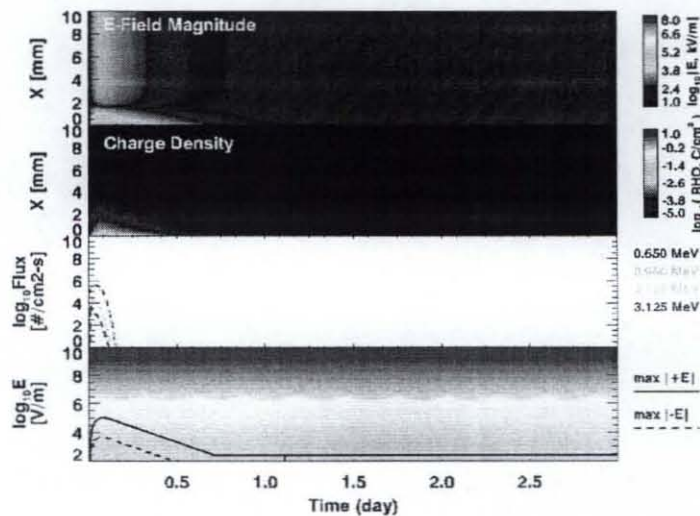
10th SCTC 18-22 June 2007
Biarritz, France

25



Lunar Transit

- 60 deg inc
- AE-8 max
- Material 2



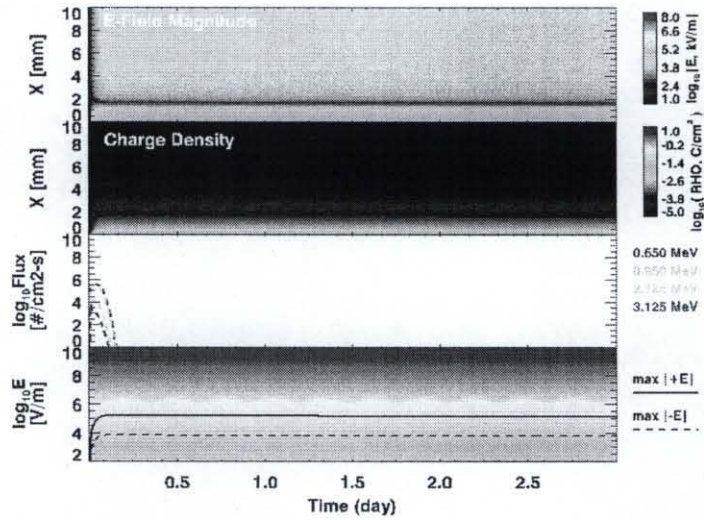
10th SCTC 18-22 June 2007
Biarritz, France

26



Lunar Transit

- 60 deg inc
- AE-8 max
- Material 3



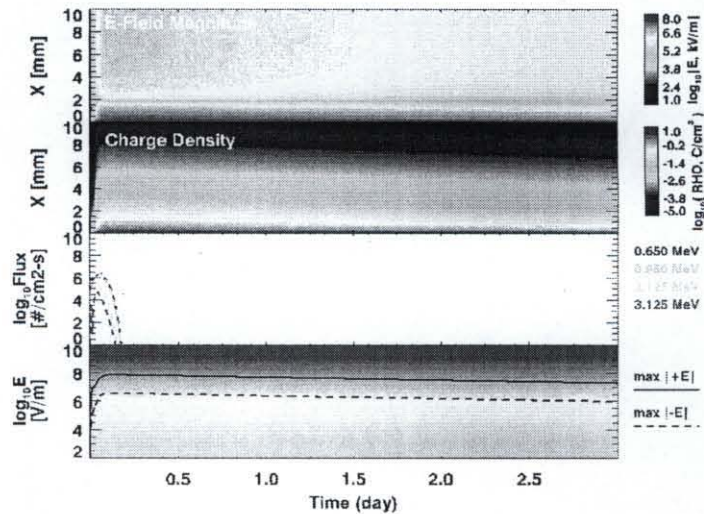
10th SCTC 18-22 June 2007
Biarritz, France

27



Lunar Transit

- 30 deg inc
- AE-8 max
- Material 4



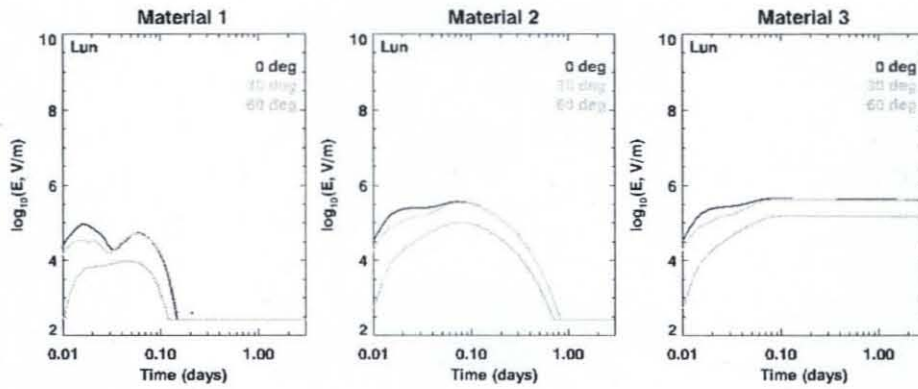
10th SCTC 18-22 June 2007
Biarritz, France

28



Lunar Transit

- Maximum electric field

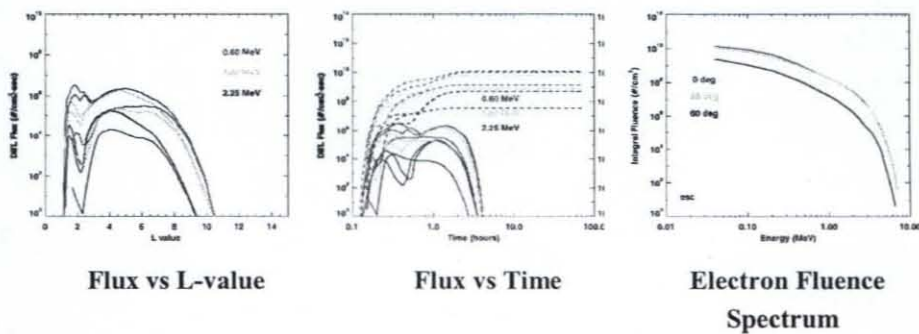


10th SCTC 18-22 June 2007
Biarritz, France

29



Earth Escape



AE-8 solar maximum

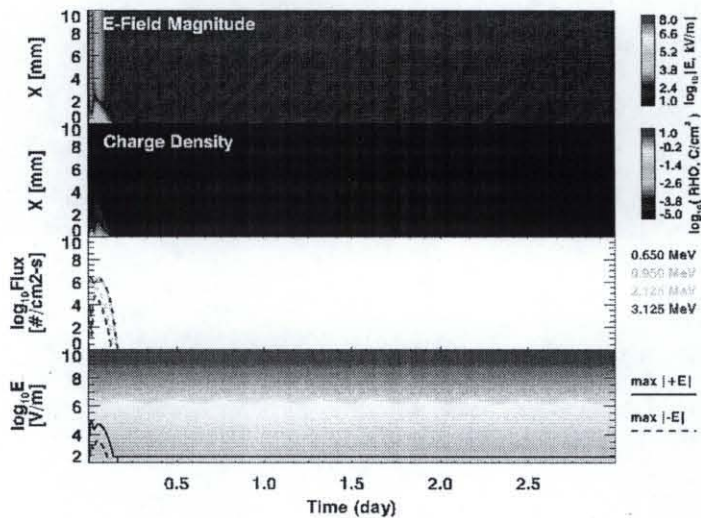
10th SCTC 18-22 June 2007
Biarritz, France

30



Earth Escape

- 0 deg inc
- AE-8 max
- Material 1

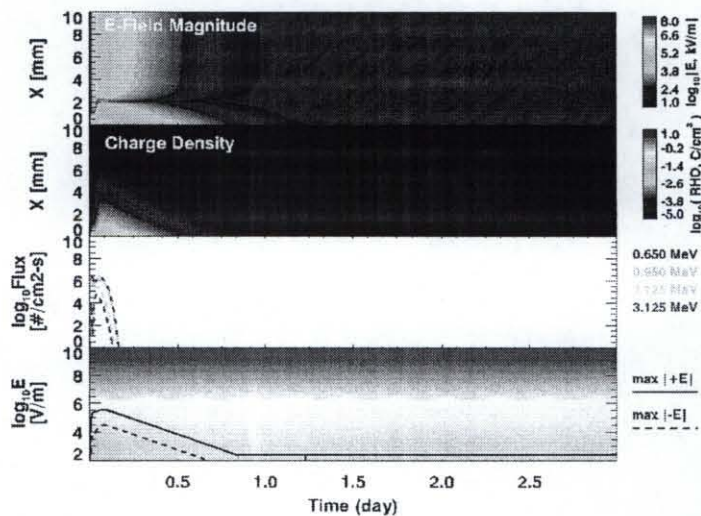


31



Earth Escape

- 0 deg inc
- AE-8 max
- Material 2

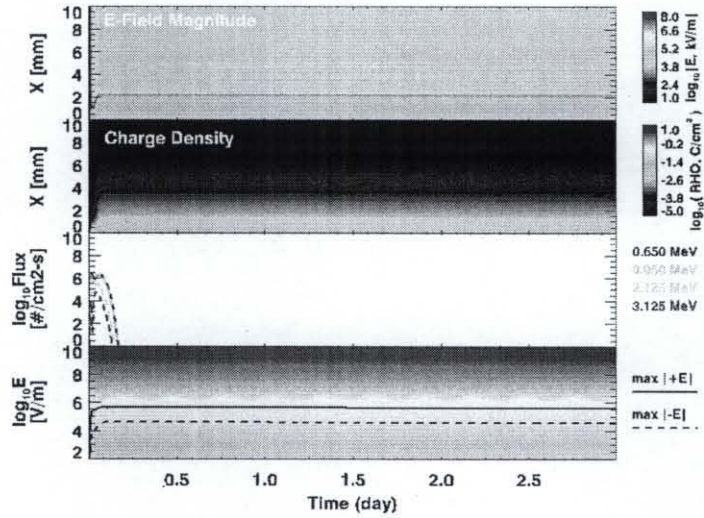


32



Earth Escape

- 0 deg inc
- AE-8 max
- Material 3



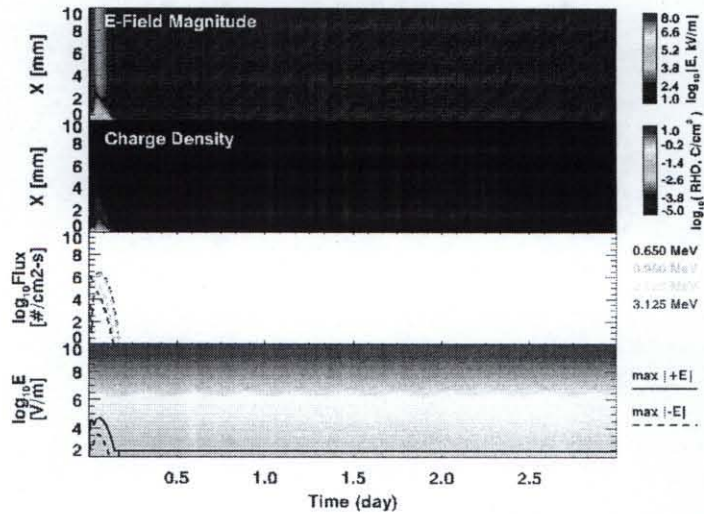
10th SCTC 18-22 June 2007
Biarritz, France

33



Earth Escape

- 30 deg inc
- AE-8 max
- Material 1



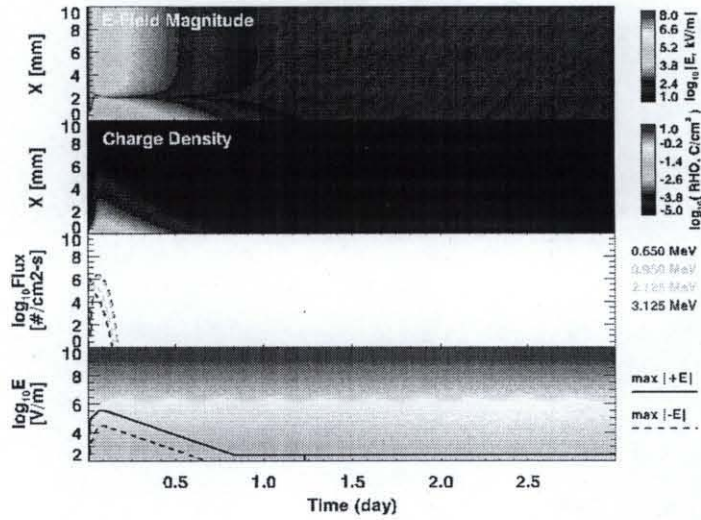
10th SCTC 18-22 June 2007
Biarritz, France

34



Earth Escape

- 30 deg inc
- AE-8 max
- Material 2



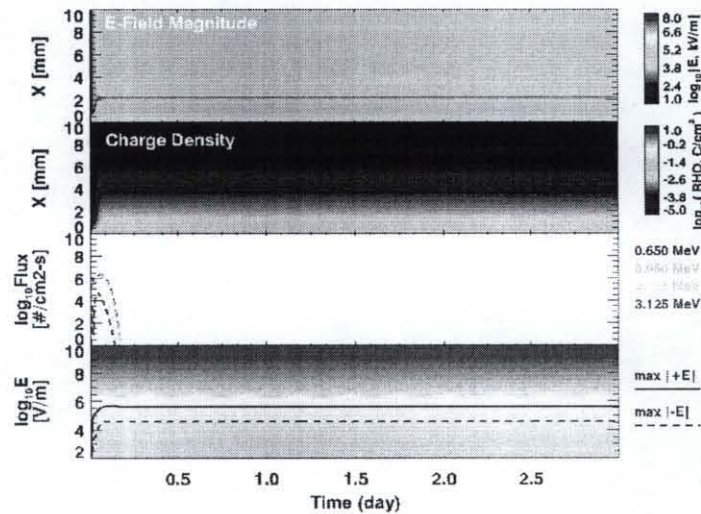
10th SCTC 18-22 June 2007
Biarritz, France

35



Earth Escape

- 30 deg inc
- AE-8 max
- Material 3



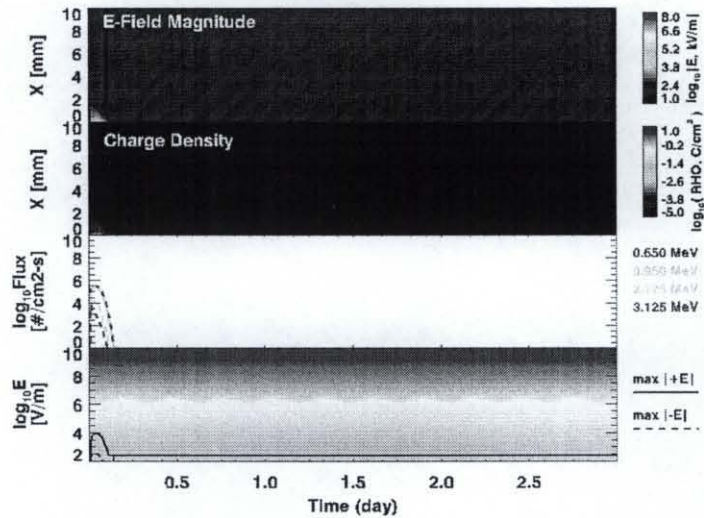
10th SCTC 18-22 June 2007
Biarritz, France

36



Earth Escape

- 60 deg inc
- AE-8 max
- Material 1



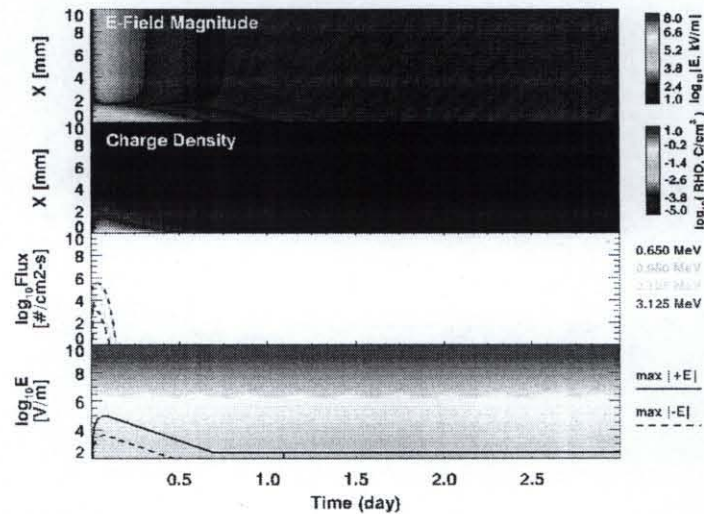
10th SCTC 18-22 June 2007
Biarritz, France

37



Earth Escape

- 60 deg inc
- AE-8 max
- Material 2



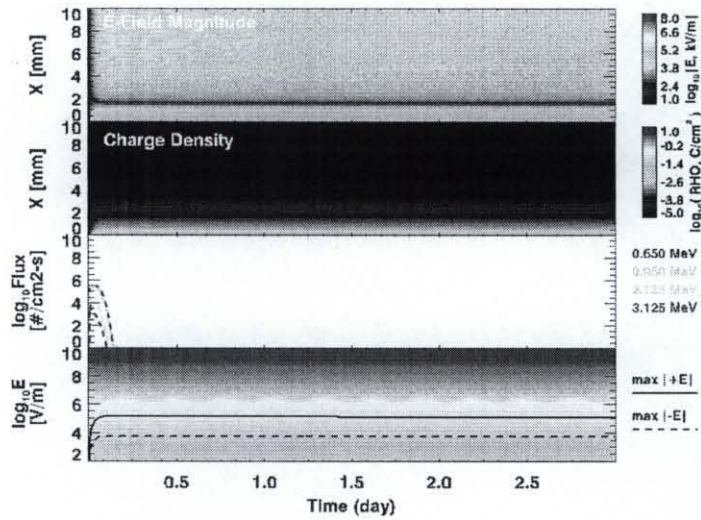
10th SCTC 18-22 June 2007
Biarritz, France

38



Earth Escape

- 60 deg inc
- AE-8 max
- Material 3



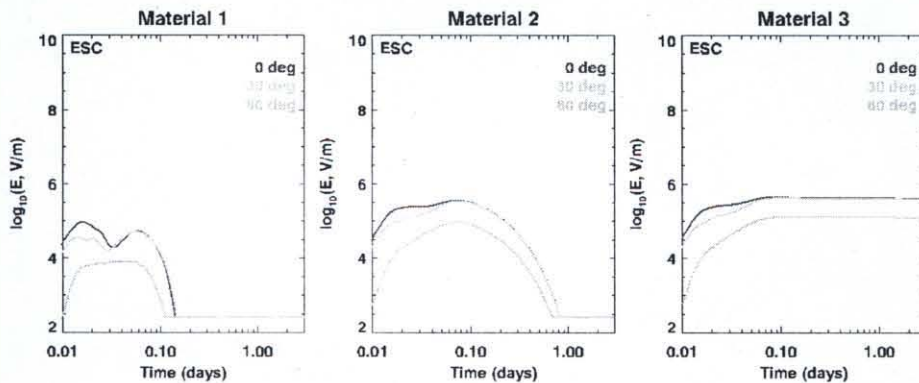
10th SCTC 18-22 June 2007
Biarritz, France

39



Earth Escape

- Maximum electric field

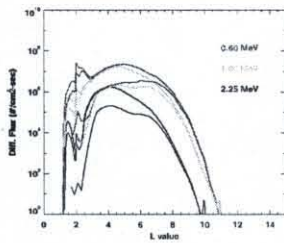


10th SCTC 18-22 June 2007
Biarritz, France

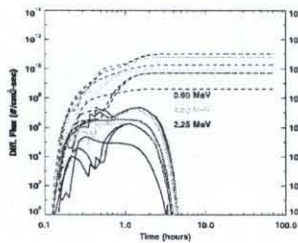
40



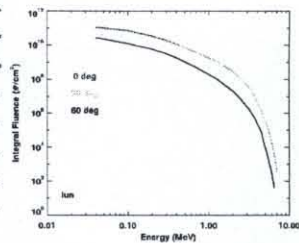
Lunar Extreme Environments



Flux vs L-value



Flux vs Time



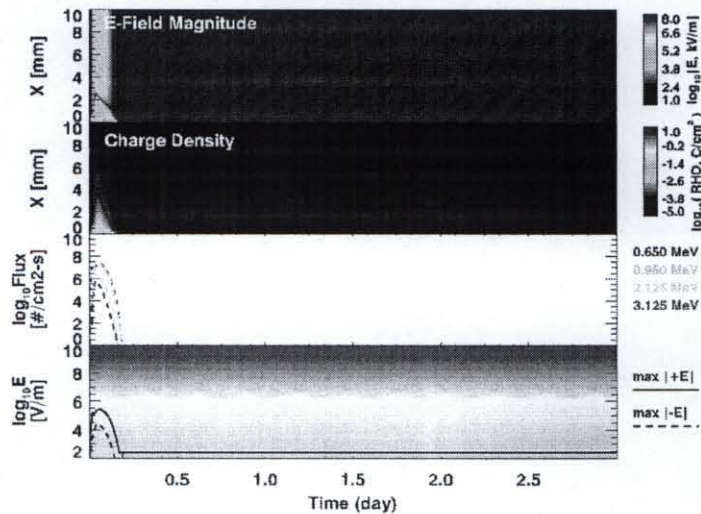
Electron Fluence Spectrum

AE-8 solar maximum



Lunar Extreme Environments

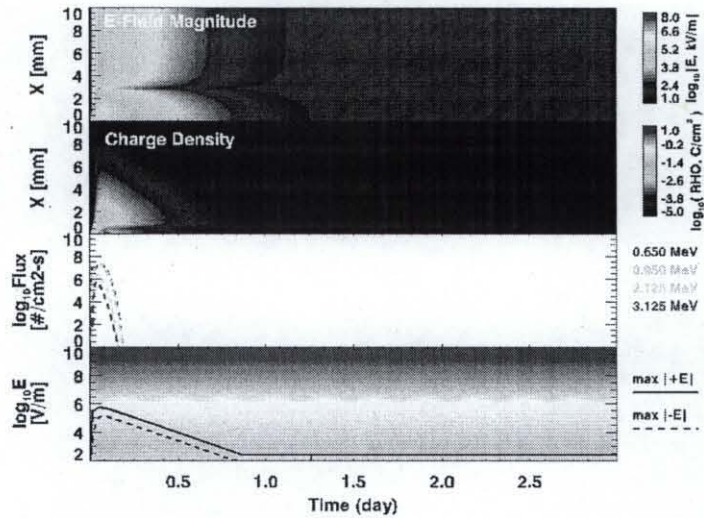
- 30 deg inc
- AE-8 max
- 10x L ≥ 2
- Material 1





Lunar Extreme Environments

- 30 deg in
- AE-8 max
- $10x L \geq$
- Material

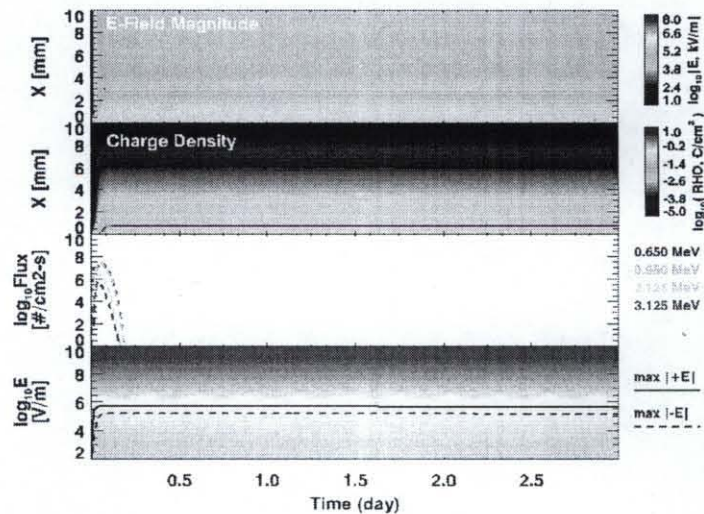


43



Lunar Extreme Environments

- 30 deg in
- AE-8 max
- $10x L \geq$
- Material

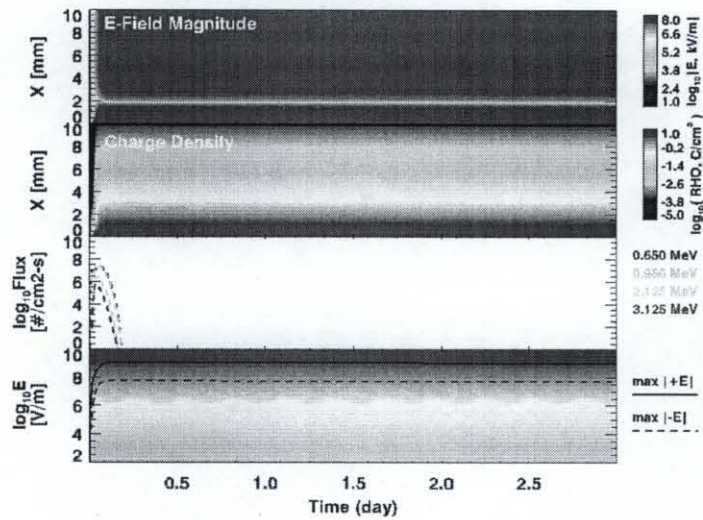


44



Lunar Extreme Environments

- 30 deg inc
- AE-8 max
- $10x L \geq 100$
- Material



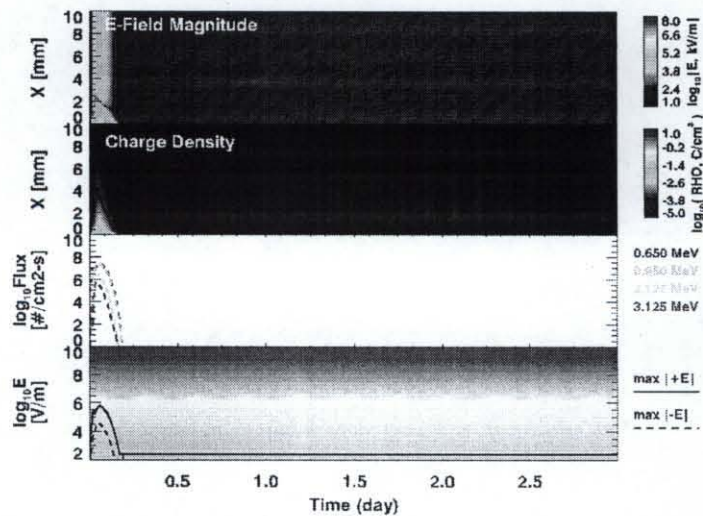
10th SCTC 18-22 June 2007
Biarritz, France

45



Lunar Extreme Environments

- 30 deg inc
- AE-8 max
- $10x L \geq 100$
- Material



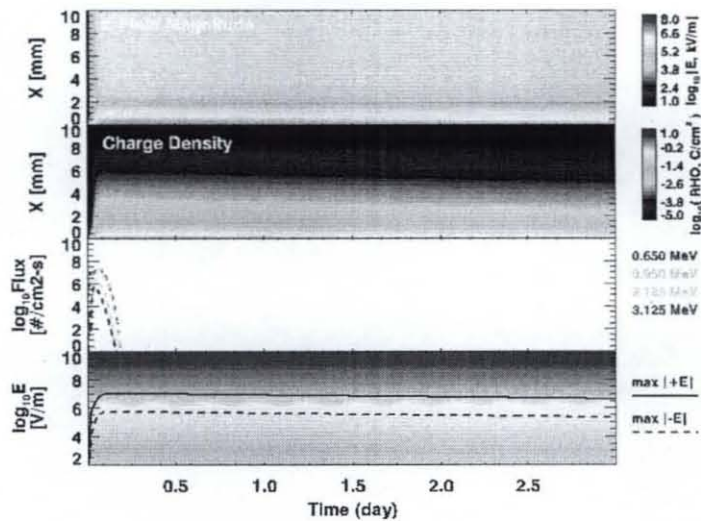
10th SCTC 18-22 June 2007
Biarritz, France

46



Lunar Extreme Environments

- 30 deg inc
- AE-8 max
- 10x L ≥
- Material



47



Summary

- NUMIT modified to read in electron flux time series
- Screen charging environments for three trajectories, three materials
 - GTO
 - Lunar transit
 - Earth escape
- GTO charging results
- Earth-Moon transfer orbit charging results demonstrate need to evaluate dielectric materials for use in lunar programs.

10th SCTC 18-22 June 2007
Biarritz, France

48